Remote Sensing of Environment 198 (2017) 187–202

Contents lists available at ScienceDirect

Remote Sensing of Environment

journal homepage: www.elsevier.com/locate/rse

Characterizing hydrologic changes of the Great Dismal Swamp using SAR/InSAR

Jin-Woo Kim [a,*], Zhong Lu [a], Laurel Gutenberg [b], Zhiliang Zhu [c]

[a] Roy M. Huffington Dept. of Earth Sciences, Southern Methodist University, Dallas, TX, USA
[b] Earth Systems and GeoInformation Sciences, George Mason University, Fairfax, VA, USA
[c] U.S. Geological Survey, Reston, VA, USA

ARTICLE INFO

Article history:
Received 13 May 2016
Received in revised form 11 May 2017
Accepted 7 June 2017
Available online xxxx

Keywords:
Great Dismal Swamp
Peatlands
Groundwater level changes
SAR
InSAR
Soil moisture
SMAP

ABSTRACT

The Great Dismal Swamp (GDS), one of the largest, northernmost peatlands on the Atlantic Coastal Plain, is underlain by a thick water-logged organic soil layer (peat) made up of dead and decaying plant material. The peatland functions as a main sink for a large amount of soil derived organic carbon. The disturbance of this wetland has negatively impacted the ecosystem and contributed to climate change through the release of the stored greenhouse gases. Surface water level and soil moisture conditions are critical information about peatlands, but monitoring these hydrologic changes has been a challenging task. With a lack of in situ soil moisture measurements, we first explored yearlong Soil Moisture Active Passive (SMAP) data to find the close relationship (R-squared value: 0.80) between soil moisture and groundwater table from March 2015 to March 2016. Based on synthetic aperture radar (SAR) backscattering returns and interferometric SAR (InSAR) phase measurements from C-band Radarsat-1 and L-band ALOS PALSAR datasets, we then analyzed the hydrologic changes in the peatlands. We compared averaged C/L-band SAR backscattering intensity (mid 1998–early 2008 for Radarsat-1, late 2006–early 2011 for ALOS PALSAR) with groundwater level changes and found that the SAR backscattering is significantly responsive (R-squared value: 0.76 and 0.67 for Radarsat-1 and ALOS PALSAR, respectively) to soil moisture changes through a three-way correlated relationship of soil moisture, groundwater level, and SAR intensity. Using InSAR coherence observations, we delineated the inundated area (western and northern regions of GDS) during the wet season, subject to double-bounce backscattering. We measured the relative water level changes in the inundated areas through the InSAR phase measurements, and estimated the groundwater level changes corresponding to soil moisture changes using time-series InSAR analysis. Our comprehensive study has demonstrated that time-series SAR backscattering returns and InSAR analysis can be used to gauge soil moisture conditions and to monitor the hydrologic and vegetation changes in the GDS.

1. Introduction

A peatland is wetland with a thick water-logged organic soil layer (peat) made up of dead and decaying plant material. Peatlands cover <3% of Earth's surface area, but they contain the equivalent of half of the carbon that is in the atmosphere as CO_2 (Dise, 2009). Peatlands are unbalanced systems where production rates exceed decomposition rates, leading to the accretion of carbon, and ultimately functioning as a sink of a large amount of organic carbon (Fenner and Freeman, 2011). The Great Dismal Swamp (GDS) is one of the largest, seasonally flooded, and nonriverine swamp on the Atlantic Coastal Plain (Mitsch and Hernandez, 2013). The impounded water from seasonal flooding boosts the accumulation of the organic soils (peats) in forested wetlands that are highly acid, impermeable, and combustible. For centuries the peatland has been exposed to intense human activities and has experienced drastic changes to the ecosystem and hydrology. The swamp, not far from the first permanent English settlement in the Americas, Jamestown, Virginia, was initially developed by George Washington and drained for agricultural use in many areas. Ditches and canals were constructed throughout the swamp to promote drainage and transport harvested timber. Due to intensive development, the area has been reduced from an estimated 202,350 ha in precolonial times to 85,000 ha today (Day, 1982). Recent scientific studies have revealed vital factors effecting the disturbance and storage processes in peatlands (Fenner and Freeman, 2011; Ise et al., 2008). Hydrology is the driving force controlling most surface and subsurface processes in peatlands. The GDS is not a riparian environment, so the flooding regime is clearly the dominant influence. The frequency, timing, depth, and duration of inundation are all critical factors affecting vegetation distribution patterns and processing rates through the regulation of soil properties such as

* Corresponding author at: Roy M. Huffington Department of Earth Sciences, Southern Methodist University, 3225 Daniel Avenue, Suite 207, Dallas, TX 75205, USA.
E-mail address: jinwook@smu.edu (J.-W. Kim).

http://dx.doi.org/10.1016/j.rse.2017.06.009
0034-4257/

nutrient availability and oxygen content (Day et al., 1988). These hydrologic changes to the soil layer are a key factor in the biochemical processes regulating greenhouse gas fluxes (carbon dioxide and methane) and the storage of carbon (Ise et al., 2008).

Methane is produced in the anaerobic conditions of saturated peatlands and with shallow ground water conditions methane is released into the atmosphere. Methane emissions are reduced when the ground water surface drops, forcing the gas to travel through aerobic soils where methanotrophic bacteria consume the gas (Harriss et al., 1982; Fenner and Freeman, 2011). This relationship to ground water can influence the regulation of soil decomposition processes and greenhouse gas fluxes, and periodic, seasonal water inputs to the GDS have created an anoxic environment where decomposition of organic material is slowed, effectively storing the carbon within the saturated soils. These unique soil conditions also support a limited range of vegetation species that increase the uptake of atmospheric carbon dioxide, including Atlantic White Cedar, Cypress Gum, Maple Gum, and Pine Pocosin (Sleeter et al., 2017).

Preserving the natural hydrologic changes in peatlands is crucial for regulating the negative impacts associated with the disturbance of peat soils. Because the GDS is primarily influenced by seasonal fluctuation of surface water and groundwater flow, extensive anthropogenic drainage efforts have resulted in significant drying of the near-surface peat layers. These conditions have progressively converted the wet, organic rich soils into dry, granular soils. Soil transformations of this nature are usually irreversible and can accelerate the greenhouse gas flux and make peat soils more susceptible to natural ignition during lightning or human-ignited fires, where the peats burn through smoldering combustion. This flameless form of combustion occurs more readily than flaming combustion, but can be coupled with flaming combustion under drought conditions (Turetsky et al., 2014). The sensitivity of peatlands to hydrologic conditions in the soil and resulting contributions to climate change have been identified and defined (Ise et al., 2008), however, monitoring these hydrologic changes, such as water table and soil water content, has been a challenging task. The spatial extent of hydrologic effects can be both localized and regional, requiring substantial in situ measurements to adequately define changes taking place. The wet, remote, and expansive nature of peatlands, make in situ measurements both difficult and costly to obtain, often resulting in a lack of information.

Synthetic Aperture Radar (SAR), with all-weather and day-and-night observing capability, has become one of the best tools to monitor the freshwater wetlands in the world (e.g., Alsdorf et al., 2000, 2001; Lu et al., 2005, 2014; Lu and Kwoun, 2008; Jung and Alsdorf, 2010; Kim et al., 2009; Kim et al., 2013; Kim et al., 2014; Wdowinski et al., 2004, 2008). The SAR backscatter coefficient from a long wavelength sensor in wetlands is sensitive to soil moisture, surface inundation, vegetation type, and leaf-on/off condition. Radar waves can penetrate vegetation canopy and interact with ground surface, and thus observe the land and water surface beneath the forest canopy and soil moisture content that is correlated with groundwater table. With the capability of discriminating land cover types and delineating inundated areas in large river basins and wetland areas (Hess et al., 1990; Hess et al., 1995; Hess et al., 2003; Ramsey, 1995; Wang et al., 1995; Kwoun and Lu, 2009), SAR intensity can be used to retrieve the soil properties, such as soil moisture, for various hydrological and meteorological applications (e.g., Lu and Meyer, 2002; Kasischke et al., 2009; Kornelsen and Coulibaly, 2013). Furthermore, exploiting phase and coherence components through interferometric SAR (InSAR), we can measure the water level changes and observe the scattering characteristics of vegetation types in these wetland environments (Brisco et al., 2017; Kim et al., 2009; Jung and Alsdorf, 2010; Kwoun and Lu, 2009; Kim et al., 2013; Kim et al., 2014; Lu and Kwoun, 2008; Ramsey et al., 2006).

There has been a strong interest to find the correlation between SAR observations and soil moisture changes through analyzing hydrologic condition in land surfaces where human disturbance (i.e. drainage, deforestation) has put constant pressure on the environmental condition. There have also been numerous efforts to observe the soil moisture in agricultural fields, bare soil fields (Dubois et al., 1995; Le Hégarat-Mascle et al., 2002; Moran et al., 2000; Oh et al., 1992), and vegetation-covered regions (Ulaby et al., 1982; Romshoo et al., 2002; Wigneron et al., 2004; Joseph et al., 2010). Most of these studies relied on SAR backscatter models that utilized low/high order polynomials or exponential and logarithmic equations, that were defined from in situ soil moisture, biomass, and roughness measurements. However, the equations differ from sensor to sensor and site to site, and the SAR backscattering, particularly from spaceborne sensors, is heavily influenced by artifacts from speckles and noise. The coherent contribution of the returned SAR signal comes from independent scatterers randomly distributed in the range cell (e.g., Franceschetti et al., 1992), and the speckle can include the effects of diverse backscattering mechanisms induced by soil moisture, inundation conditions, and vegetation characteristics. To overcome such limitations, the interferometric phases with high coherence can been utilized to estimate moisture changes in bare soils and beneath vegetation. A recent study found that the interferometric phases from InSAR are highly correlated with soil moisture (Zwieback et al., 2015), and the phase consistency in triplets of interferograms was introduced for soil moisture estimation (De Zan et al., 2014).

In our study, the hydrologic changes in the GDS, composed of changes in the surface water and groundwater levels, are related to soil moisture variations. These changes were observed using C- and L-band SAR time-series change analysis in the backscatter coefficients and interferometric phase in low-lying peatlands. We adopted a top-down approach, from a large scale (the entire GDS area), to an intermediate scale (areas according to vegetation covers), and finally at a small scale (a point target in a non-inundated area). This method is adopted to reduce scale related limitations, for example the SAR products, at a large scale, cannot exclude the effect of surface water, but measurements, at a smaller scale in the non-inundated regions, are relatively independent of standing surface water and mostly influenced by changes in soil moisture. Exploiting all available data products (SAR intensity as well as interferometric phase and coherence) from SAR and InSAR maximizes the utility of the spaceborne SAR sensor, and provides better definitions of the spatiotemporal hydrologic changes beneath vegetation and delineations of the areas subject to the impoundment of surface water.

2. Characteristics of study region and data

2.1. Characteristics of study region

The GDS is located on the coastal plain in southeastern Virginia and northeastern North Carolina. The surface gradient is gradual and to the east with soils that consist of unevenly distributed mucky peat underlain by clay over a shallow aquifer (Day, 1982). Once peat covered, most of the swamp floor consisted of oak and hickory forests, but has slowly been replaced by gum, cypress, juniper, and a variety of other species (Bradley, 2013). The western part of the swamp is covered by Cypress Gum (Fig. 1(a, b)), which is a typical southern swamp community adapted to surface inundation for at least part of the growing season. This forest community, covering 12% of the wetland, prospers where standing water is abundant. Cypress Gum forests are characterized by frequent, prolonged flooding from January to June, on poorly drained soils. They are slowly growing, but long-living in comparison to the other forest communities in the GDS, reaching their maximum height at 200 years (average canopy height is 30–35 m). Mortality can occur naturally any time after 200 years, but disturbance often shortens this life span (Sleeter et al., 2017). In the GDS, the Cypress Gum forest, formerly the most extensive association in the swamp, has been transformed into Maple Gum forests due to the change of the hydrologic settings and the intrusion of outside species. The Maple Gum forests,

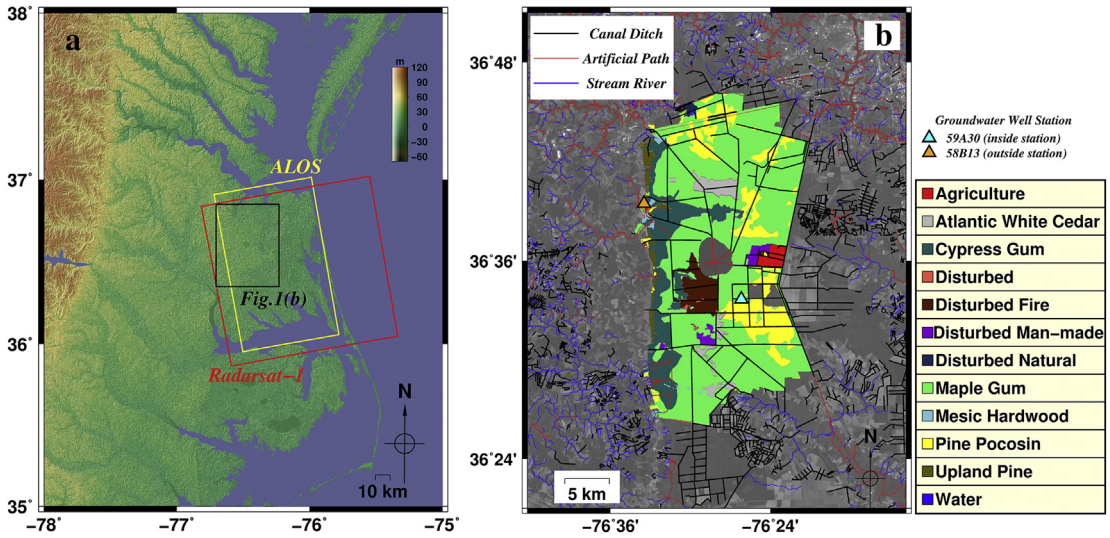

Fig. 1. (a) Shaded-relief image of the study area. The red and yellow rectangular outlines respectively show the coverage of Radarsat-1 and ALOS PALSAR images used in this study (Fig. 3). The black rectangle is the location outline for panel (b). (b) Vegetation cover map over the Great Dismal Swamp. The vegetation cover map was created by both the field inventory and formal classification of vegetation types from multi-state regional data sets available at the Virginia Department of Conservation and Recreation (Fleming et al., 2001). Lines represent streams, artificial paths, and canal ditches. Cyan triangle (59A30) and Orange triangle (58B13) are two groundwater well sites inside and near the wetland, respectively. (For interpretation of the references to color in this figure legend, the reader is referred to the web version of this article.)

currently the most dominant association, covering approximately 61% of the landscape (Fig. 1(b)), expanded over the past 30 to 40 years and are susceptible to occasional seasonal flooding (USFWS, 2006). Red Maple, one of two primary tree species of Maple Gum along with Black Gum, is a hardwood species that is native to a wide region in North America, ranging from Newfoundland in the north, to Florida in the south, and as far northwest as Illinois and southwest to Texas (Little, 1979). Red Maple can grow in conditions ranging from poor dry soils to humid wetlands. Because of its high adaptability to a wide range of site conditions, the Maple Gum can prosper in the GDS. The life span of Maple Gum is shorter than other forest communities, reaching full maturity at 70–80 years, and rarely existing beyond 150 years. Average mature trees are 18–27 m in height and 46–76 cm in DBH (diameter breast height) (Sleeter et al., 2017; Hutnick and Yawney, 1961). The Atlantic White Cedar forests are another notable community that occur sparsely along canal ditches; the forests in the westernmost part of the GDS have been transformed to upland forests due to drainage for agricultural use and now provide an ideal environment for this species. Atlantic White Cedar covers 3% of the GDS and favorable conditions for the forest community are considered stressful for other conifer species. The conditions include 4–6 months annually of water inundation, a shallow water table averaging 10 cm from the surface during the growing season, and highly acidic soils. Atlantic White Cedar can reach heights of 15–20 m and 25 cm at DBH in 50 years (Schroeder and Taras, 1985). The Pine Pocosin occurs in areas where organic soils have poorly developed internal drainage, and the low-lying vegetation is dominated by broadleaved evergreen shrubs with average heights of 14 m and DBH of 25 cm (USFWS, 2006). Biophysical characteristics of the species vary based on peat depth, soil saturation, and fire history. The height of Pine Pocosin increases with decreasing peat depth (Sleeter et al., 2017). In contrast to other forested wetlands, Pine Pocosin is a lone shrubland in the GDS. The disturbed classes (Fig. 1(b)) are defined as the areas damaged by wildfires (Disturbed Fire), anthropogenic developments (Disturbed Man-made), tropical storms (Disturbed Natural) or unidentified causes (Disturbed). Among all communities in the GDS (Fig. 1(b)), Cypress Gum is the most susceptible to the seasonal surface water impoundment, followed by Atlantic White Cedar, and then Pine Pocosin. Surface water covering the areas populated by Cypress Gum is abundant during wet seasons due to local topography and close proximity to the hydrologic inputs, while the Pine Pocosin have little to no standing surface water. Upland Pine, growing in the westernmost areas of the GDS, experiences barely any inundation during the high-water season, and the communities often occur on land that has been drained for agricultural uses.

The hydrology in the GDS can be characterized by drastic, seasonal, and multifaceted fluctuations that surface water flow from adjacent upland areas, rainfall, evapotranspiration, and outflows in ditches and river/stream channels. Usually in wetlands, the season with the greatest amount of precipitation is anti-correlated with the season that experiences high water. However, in the GDS, despite the large amount of rainfall in the summer, this is the lowest water season (Carter et al., 1977). Because of the atmospheric regimes in the GDS during this season, the evapotranspiration exceeds rainfall and becomes the biggest source of water removal (USFWS, 2006). The discharge through ditches, river channels, and the Dismal Swamp Canal consistently contribute to the water outflow year round. In the winter, when the evapotranspiration becomes less influential, surface runoff is apparent across the entirety of the swamp with flooding and overflowing ditches and canals typical in the western and northern regions of the wetland. This flooding provides significant benefits in the peatland environment by preserving the appropriate soil moisture throughout the year and suppling the ecosystem with necessary nutrients.

2.2. Data

C-band (wavelength of 5.7 cm) Radarsat-1 and L-band (wavelength of 23.6 cm) ALOS PALSAR datasets were used for this study. A total of 31 standard beam mode Radarsat-1 images from May 1998 to April 2008 (red box of Fig. 1(a)) were utilized for our study. Radarsat-1 has a HH polarization with a spatial resolution of 30 m at this beam mode. In addition, 13 fine beam mode ALOS PALSAR images from 2006 to 2011 (yellow box of Fig. 1(a)) were acquired. Among the PALSAR images, four were acquired in Fine Beam Single-polarization (FBS) model with HH polarization. The rest of the PALSAR scenes were in Fine Beam Dual-polarization (FBD) mode which includes both HV and HH polarizations. HV polarized SAR images are effected by volume scattering and are not preferred for studying wetland hydrology beneath forest canopy (Lu et al., 2005, 2014; Lu and Kwoun, 2008; Kim et al., 2009). Thus, only HH polarized SAR images from both satellites were applied to our study because this polarization is relatively independent of volume scattering and is instead sensitive to double-bounce backscattering in forested wetlands (Lu and Kwoun, 2008; Kim et al., 2009).

The lack of adequate hydrological field measurements to provide a means of ground-truthing the remotely acquired SAR data presents challenges in studying the GDS. Surface water level and soil moisture measurements are critical information to monitor the health and evolution of peatlands and provide information to use as comparison to remotely sensed data. Unfortunately, in the GDS most water gages are only located along ditches and canals. Because the water flow near these artificial structures cannot fully reflect the hydrologic changes throughout the swamp, the gauged measurements are not compared with our SAR and InSAR measurements. Additionally, there were no permanent stations to measure soil moisture inside the swamp. Soil Climate Analysis Network (SCAN) provides one of the largest soil moisture networks in the U.S., but the SCAN stations are dense in Utah, Nevada, California, and Mississippi leaving the eastern U.S. with limited coverage. We instead had to exploit information about the groundwater table from groundwater sites operated by U.S. Geological Survey (USGS). Somorowska (2003) proposes that the depth of the water table, defined as the measurement from the ground surface to the top of the groundwater, is closely associated with soil moisture content. This hypothesis needs to be confirmed by ground-truth or supplementary data, because wetlands involve a variety of different environmental settings that can produce individual responses between groundwater fluctuation and soil moisture. To assess this relationship, we employed the products available from the Soil Moisture Active and Passive (SMAP) satellite that was launched in January 2015 with global soil moisture measurements available from late March 2015 to the present. NASA's SMAP mission planned to use L-band SAR and a radiometer to concurrently estimate soil moisture that can then be integrated as a single observation system. The combination of active (SAR) and passive (radiometer) sensor produces a synergistic effect while improving resolution and maintaining high sensitivity to soil moisture, surface roughness, and vegetation scattering (NASA, 2014). Although the active SAR sensor stopped operating due to a power failure in July 2015, the SMAP's radiometer-derived products still offer a unique opportunity to remotely measure wetland soil moisture (particularly in the top 5 cm of the soil column) from space. From a variety of SMAP products, we selected Level 4 surface soil moisture measurements to compare with the groundwater level. The SMAP Level 4 soil moisture products are estimated by assimilating a land surface model that monitors the evolution of soil moisture, snow, temperature, and precipitation, with the SMAP observations that are weighted by the uncertainties in both the satellite data and land model predictions (NASA, 2014). The nominal resolution of Level 4 SMAP surface soil moisture data (unit: m^3/m^3) is 9 km.

In addition, we utilized the groundwater level from two gage stations (groundwater wells) in our study area: one inside the swamp (cyan triangle in Fig. 1(b), hereafter called inside station) and one outside the swamp (orange triangle in Fig. 1(b), hereafter called outside station). These inside and outside stations were installed in 2009 and 1981, respectively. Despite the decadal difference in installation, measurements of these gage stations are considered reliable because the data exhibit subtle and consistent sensitivities to the seasonal hydrologic fluctuations expected in the wetland and provide magnitudes that are in good agreement with each other. For long-term comparison of SAR intensity analysis, the data from the outside station were utilized. The measurements from the inside station were compared with results from InSAR time-series analysis spanning from 2009-present and used to assess the relationship between SMAP surface soil moisture and groundwater level.

3. Methodology

In general, radar backscattering in forested wetlands represents a combination of surface, double-bounce, and volume scatterings. Over bare-earth or agricultural fields, the backscattering mechanism is relatively simple and is dominated by surface scattering with little or no penetration. Backscattering over forested wetlands, such as the GDS, depends upon numerous factors, including the vegetation cover and density, soil moisture content, aboveground biomass, canopy opening, and the level of standing water in areas that are flooded. For example, when the swamp is flooded during the wet season, double-bounce scattering is magnified and SAR backscattering is thereby strong, but this effect can differ with the vegetation cover. In relatively low-lying peatlands covered by shrubs, the double-bounce scattering will be weak compared to taller Cypress-covered forests. Analysis relying completely on the SAR backscatter cannot exclude the effects of seasonal inundation and double-bounce scattering from standing surface water in the vegetated peatland. Vegetation cover can provide complimentary information such as the Upland Pine or Pine Pocosin is less influenced by the presence of seasonal standing water compared to Cypress Gum and Maple Gum. Using this data in comparison with the SAR backscatter and gage measurements of the local groundwater levels can help find the relationship between the SAR backscattering and the soil moisture. In addition, it should be noted that the SAR backscattering intensity values include the speckle effects due to the coherent sum of backscattered signals from multiple distributed targets. Hence, we averaged the SAR intensity over the whole GDS according to the vegetation cover, and compared the averages with groundwater level measurements.

Comparison between direct soil moisture measurements and the SAR products (SAR backscatters and interferometric phases) is optimal for establishing their relationship and identifying causes for variations in the radar measurements. We do not, unfortunately, have long term ground-truth measurements of soil moisture and there are no temporal overlaps between spaceborne observations (i.e. SMAP soil moisture from March 2015 to March 2016 and SAR backscatters (Radarsat-1 and ALOS PALSAR) from 1998 to 2011). When we consider the seasonal and inter-annual fluctuations of soil moisture and radar measurements, direct comparison of different temporal periods is clearly inappropriate. Therefore, a three-way comparison of soil moisture measurements, groundwater level changes, and our SAR products was employed. If there is a close relationship between soil moisture variations and groundwater level changes, we can infer the association between soil moisture and SAR backscattering returns. The latest observation of SMAP provided us with a time-series of soil moisture measurements from space and although the Level 4 products have a coarse grid size of 9 km (Fig. 2(a)), which includes undesired effects from nearby agricultural fields, the overall temporal variations should be closely related to the soil moisture changes in the GDS. Fourteen 9-km Equal-Area Scalable Earth-2 (EASE2) grids (Brodzik et al., 2012) from Level 4 SMAP products cover the GDS (Fig. 2(a)), but a single grid (blue box of Fig. 2(a)), where weather station (yellow triangle) and groundwater well (cyan triangle) exist, was selected to compare the soil moisture with the groundwater level.

The coherence and interferometric phase are two major products of InSAR processing. InSAR coherence can be calculated by cross-correlation of the co-registered SAR image pair over a small window of pixels (Lu and Freymueller, 1998; Lu and Dzurisin, 2014):

$$\gamma = \left| \frac{\sum C_1 C_2^*}{\sqrt{\sum |C_1|^2 \sum |C_2|^2}} \right| \quad (1)$$

where C_1 and C_2 are complex-valued backscattering coefficients, and C_2^* is the complex conjugate of C_2. Coherence represents the consistency of scattering mechanisms between two pixels with the same location but acquired at different times. If the surface condition is altered or the area has dense vegetation, the coherence becomes low. Wavelength is a key factor in coherence estimate: L-band SAR signal with a long wavelength (23.6 cm) can keep high coherence in forested wetlands while the shorter wavelength of C-band data (5.7 cm) cannot penetrate the canopy and thus loses coherence. Generally, when the primary focus is estimating surface water level change using techniques in InSAR

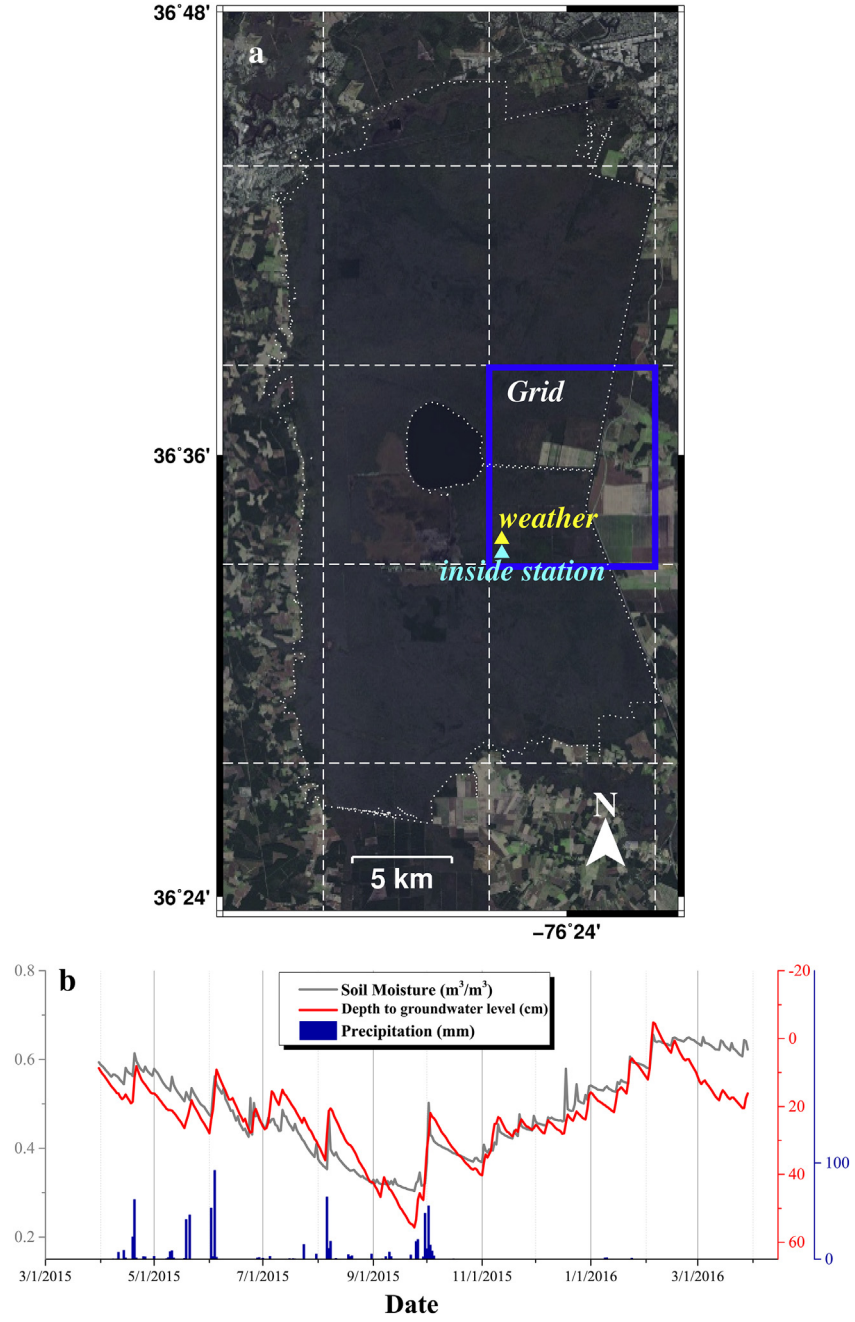

Fig. 2. (a) 9-km SMAP grid around the GDS. The blue box outlines the area where Level 4 time-series SMAP surface soil moisture values were obtained to be used in comparison with groundwater level measurements from a USGS well (cyan triangle: inside station of Fig. 1) and precipitation that was recorded at the nearby weather station (yellow triangle). (b) Time-series SMAP soil moisture (gray line) and groundwater level (red line) during a year (2015.03.31–2016.03.29). Blue bar graph represents precipitation for the same period. (For interpretation of the references to color in this figure legend, the reader is referred to the web version of this article.)

processing, the data with low coherence are considered useless. However, the spatial variation of coherence also provides useful information on flooding condition and vegetation cover (Kwoun and Lu, 2009). Based on InSAR coherence, we can delineate the areas inundated with surface water in the vegetated wetlands because swamp forests and marshes or bogs covered with tall shrubs tend to maintain high coherence during the high water (wet) seasons. Using these characteristics, the regions unaffected by standing water and run-off events can be extracted to better compare the relationship between soil moisture changes and InSAR products. The interferometric phase change observed over wetland environments has also been used to estimate relative water level changes (e.g., Alsdorf et al., 2000, 2001; Kim et al., 2009). Increases in the stream, canal, and subsurface discharge rates during the wet season have large impacts on the hydrologic storage and movement in the GDS that can result in surface run-off events near the inflow of ditches and streams. Therefore, InSAR can estimate the localized relative water level changes in the sections dissected by ditches, following the equation:

$$\partial h = -\frac{\lambda \phi_{def}}{4\pi \cos\theta} + n \tag{2}$$

where ∂h is relative water level change, θ is an incidence angle, λ is the wavelength, ϕ_{def} is deformation phase after differential InSAR processing, and n is a noise component. Furthermore, when we have results from processing InSAR time-series, we can estimate temporal variations of surface deformation. Based on the Small BAseline Subsets (SBAS)

algorithm (Berardino et al., 2002; Schmidt and Bürgmann, 2003), we can calculate time-series vertical displacements from multiple interferograms using the equation:

$$\begin{bmatrix} 0 \\ \phi_{1,2} \\ \phi_{1,5} \\ \phi_{2,5} \\ \cdots \\ \phi_{i,j} \end{bmatrix} = -\frac{4\pi}{\lambda}\cos\theta \begin{bmatrix} 1 & 0 & 0 & 0 & 0 & \cdots & 0 \\ -1 & 1 & 0 & 0 & 0 & \cdots & 0 \\ -1 & 0 & 0 & 0 & 1 & \cdots & 0 \\ 0 & -1 & 0 & 0 & 1 & \cdots & 0 \\ \cdots & \cdots & \cdots & \cdots & \cdots & \cdots & \cdots \\ 0 & 0 & -1 & 0 & 1 & \cdots & 0 \end{bmatrix} \times \begin{bmatrix} d_1 \\ d_2 \\ d_3 \\ d_4 \\ \cdots \\ d_{N+1} \end{bmatrix} \quad (3)$$

where $\phi_{i,j}$ is interferometric phase between i and jth SAR obervations, d_i is the ith cumulative vertical component (deformation) in time order, and N is the number of SAR acquisitions. When there are time-series interferometric phase changes in non-inundated areas, they can be related to moisture changes in the upper soil columns (Zwieback et al., 2015). Therefore, at a small-scale, for a target area that is vegetated but not inundated all year, time-series interferometric phases and soil moisture changes (via groundwater level changes) will be compared.

4. Results

4.1. Relationship between soil moisture and groundwater level changes

Because SMAP products have only been released since March 31, 2015, year-long datasets (March 31, 2015 to March 29, 2016) of SMAP soil moisture, groundwater level, and precipitation were analyzed. The majority of the precipitation for this area occurs between April and October (blue bars in Fig. 2(b)), and the expected correlation of associated increases in the soil moisture and groundwater level with increased precipitation are clearly observed (gray and red lines, respectively in Fig. 2(b)).

Precipitation is thus verified to be a driver of increases in soil moisture and groundwater levels (USFWS, 2006; NASA, 2014). The groundwater and soil moisture data also indicate summer to be the driest season, with the lowest soil moisture and groundwater levels occurring in September, because evapotranspiration throughout the summer has removed significant amounts of water from both the surface and underground (USFWS, 2006) (Fig. 2(b)). Despite low precipitation after October, soil moisture increased during the winter, which could be attributed to weakened evapotranspiration as atmospheric temperatures drop (USFWS, 2006), but there is also an increase in groundwater level that is most likely also influential on the observed change in soil moisture. Overall, the soil moisture from SMAP and the groundwater level are highly correlated (R-squared value: 0.80 significant at $p <$ 0.001, n (number of samples): 364, ε (standard error): 0.04, intercept: 0.67 $\pm$ 0.10 (95% confidence), slope: 7.8e−03 $\pm$ 4.0e−03 (95% confidence)) for most time of the year. Based on this close relationship between soil moisture and groundwater level in the GDS, we can equate comparisons of groundwater level changes with SAR backscattering intensities and comparisons of soil moisture changes with SAR backscattering intensities. With this correlation established we can now explore how groundwater levels change in relationship to backscattering characteristics as the last segment of the three-way comparison.

4.2. Relationship between SAR intensity and groundwater level changes

The hydrologic changes in the GDS affect the SAR backscatter returns during both high water (winter) and low water (summer) seasons. Regardless of the operating radar wavelength SAR intensity images acquired in wet and dry seasons exhibit obvious differences. C-band Radarsat-1 and L-band ALOS PALSAR intensity images obtained on 01/26/2007 (Fig. 3(a)) and 12/22/2006 (Fig. 3(c)), respectively, exhibit strong radar returns due to increased double-bounce backscattering, particularly over the northern and western GDS. This area is close to the inflow of streams and ditches, and during the wet season flooding causes these channels to fill and run-off inundates the flat surfaces of the forested wetlands. However, the Radarsat-1 (Fig. 3(b)) and ALOS PALSAR images (Fig. 3(d)) acquired in the summer look much darker when compared with the SAR intensity images obtained in the wet season. As previously mentioned, the water removal caused by the summer evapotranspiration and continuous discharge through ditches contributes to the observed difference. Visual inspection of the SAR intensity images indicates that the HH polarized SAR signals are capable of penetrating the forest canopy and reaching the ground surface to interact with soil layers.

When we have SAR intensity time-series from C- and L-band sensors, we can compare the averaged SAR intensity over the GDS with the groundwater level or surface water level measurements. The water level measured in gages located along rivers and ditches does not reflect hydrologic changes inside the swamp, as inundation over flat surfaces lags behind the fast-changing surface water movements in directed channels (Kim et al., 2009). This explains why the measured surface water level from these gages did not have a high correlation with averaged SAR intensity. On the other hand, the groundwater table changes at well sites had a close relationship with changes observed in SAR intensity images. A long-term time-series of C-band Radarsat-1 SAR intensity returns from images acquired from 1998 to 2008 were averaged over the whole GDS, excluding human-disturbed areas. A positive correlation between these intensity values and the groundwater level is observed as intensity increases with the rising groundwater (Fig. 4(a)). If we focus on the time frame from 2006 to 2008, due to the sparse Radarsat-1 acquisition before 2006, this high correlation becomes obvious (Fig. 4(b)). In many wetlands the seasonal vegetation change can be influential on SAR intensity, but the SAR intensity acquired in the same season should have similar values (e.g., Kwoun and Lu, 2009). When this is performed in the GDS, SAR backscatter acquired in January of 2007 and 2008 have an evident difference with a drop of as much as 2 dB (decibel) in 2008. This means that a seasonal vegetation change is not responsible for the observed change in the forested swamp. This effect is caused by a drop in the groundwater level of 2 m between these two periods, and the related soil moisture change contributed to the observed variation in SAR intensity.

The R-squared value from a linear regression between groundwater level and C-band SAR intensity was 0.76 (R-squared value is significant at $p <$ 0.001, n: 30, ε: 0.32, intercept: −0.26 $\pm$ 0.47 (95% confidence), slope: −0.71 $\pm$ 0.16 (95% confidence)), indicating high correlation between the two parameters (Fig. 4(c)). The mean and standard deviation plot (calculated based on Kasischke and Fowler, 1989; Fig. 4(d)) shows that the low mean values of SAR intensity (during the dry season) maintained small standard deviations and high SAR intensity returns (during the wet season) had high standard deviations. This was due to the effect of combined scattering over heterogeneous vegetation cover (e.g. swamp forest in the west that is flooded during the wet season and shrub land in the east that is not flooded but moistened during the wet season).

The L-band PALSAR intensity time-series results in a similar pattern (Fig. 5(a)) to the C-band Radarsat-1 observations. The groundwater level rise and resulting increase in soil moisture elevated the SAR backscatter intensities while the intensity values during the dry season decreased. The R-squared value between ground water level and L-band SAR intensity was 0.67 (Fig. 5(b); R-squared value is significant at $p <$ 0.001, n: 13, standard error: 0.61, intercept: −1.91 $\pm$ 1.75 (95% confidence), slope: −1.29 $\pm$ 0.59 (95% confidence)), and the mean and standard deviation plot (Fig. 5(c)) is comparable to that from C-band data (Fig. 4(d)).

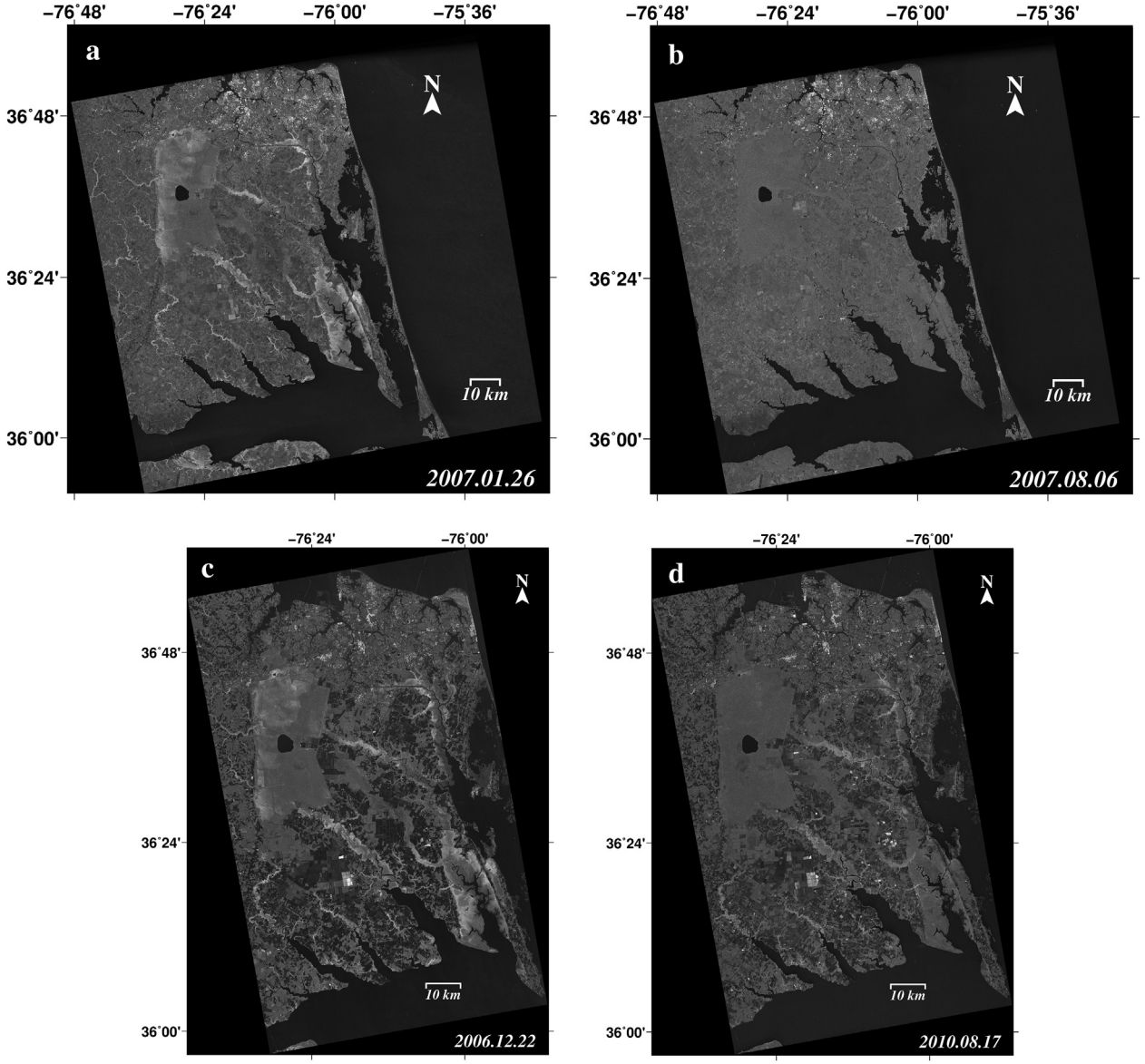

Fig. 3. Radarsat-1 SAR intensity acquired in (a) 2007.01.26 and (b) 2007.08.06. ALOS PALSAR intensity acquired in (c) 2006.12.20 and (d) 2010.08.17.

When we averaged the SAR backscattering returns according to different categories defined by vegetation cover (Fig. 6), the temporal variations follow the fluctuations of groundwater level regardless of operated radar frequency (Fig. 6(a, b, c)). Based on these results, the SAR intensities corresponding to Cypress Gum communities are the most sensitive to hydrologic changes both on the surface and within the subsurface of the forested swamp, while areas populated by Pine Pocosin were least sensitive. Nevertheless, the SAR intensity over all the vegetation types is still mostly influenced by hydrologic changes in the wetlands. Cypress Gum forests are inundated with shallow water in winter, so larger backscattering coefficients and their close relationship with groundwater levels can be attributed primarily to the double bounce scattering in the swamp forests, and to a lesser extent reflect effects of the increased soil moisture. However, other communities (Pine Pocosin and Atlantic White Cedar) are generally not submerged during wet seasons, and consequently are less influenced by the double bounce scattering. Therefore, the increased water content of the seasonally saturated soils over the shrub land and upland forests is likely the primary cause of the correlation between SAR backscattering intensity and groundwater level changes.

We are also able to identify the vegetation type defined as disturbed fire from the anomalous SAR intensity signature (red ellipse in Fig. 6(c)) observed in mid-2008 and 2009. Records indicate that a wildfire in the GDS lasted from June to October of 2008 and caused extensive damaged in the region. The burned forest and charred remnants create a rougher surface than canopy and shrub land, and this is captured by the SAR intensity data as an increase when this roughness was magnified in mid-2008 from the wildfire. After clean-up of the damaged areas (Laing et al., 2011), the SAR intensity was decreased with the new growth of vegetation in the area. The R-squared value of a linear regression between the SAR intensity averaged for each vegetation cover and the groundwater level (Table 1) highlights that most vegetation covers have strong correlations. Cypress Gum, which is the most susceptible to seasonal inundation, has larger values of 0.63, 0.81, and 0.69 for Radarsat-1 and ALOS PALSAR intensity, respectively. Maple Gum has similar values, but Atlantic White Cedar and Pine Pocosin, which are less exposed to the surface water, have smaller values for Radarsat-1 intensity. Because of this we cannot completely rule out the effect of surface water on the relationship between C-band SAR intensity and soil moisture. However, ALOS PALSAR intensity does not have considerable difference of R-squared values among major vegetation covers (Atlantic White Cedar,

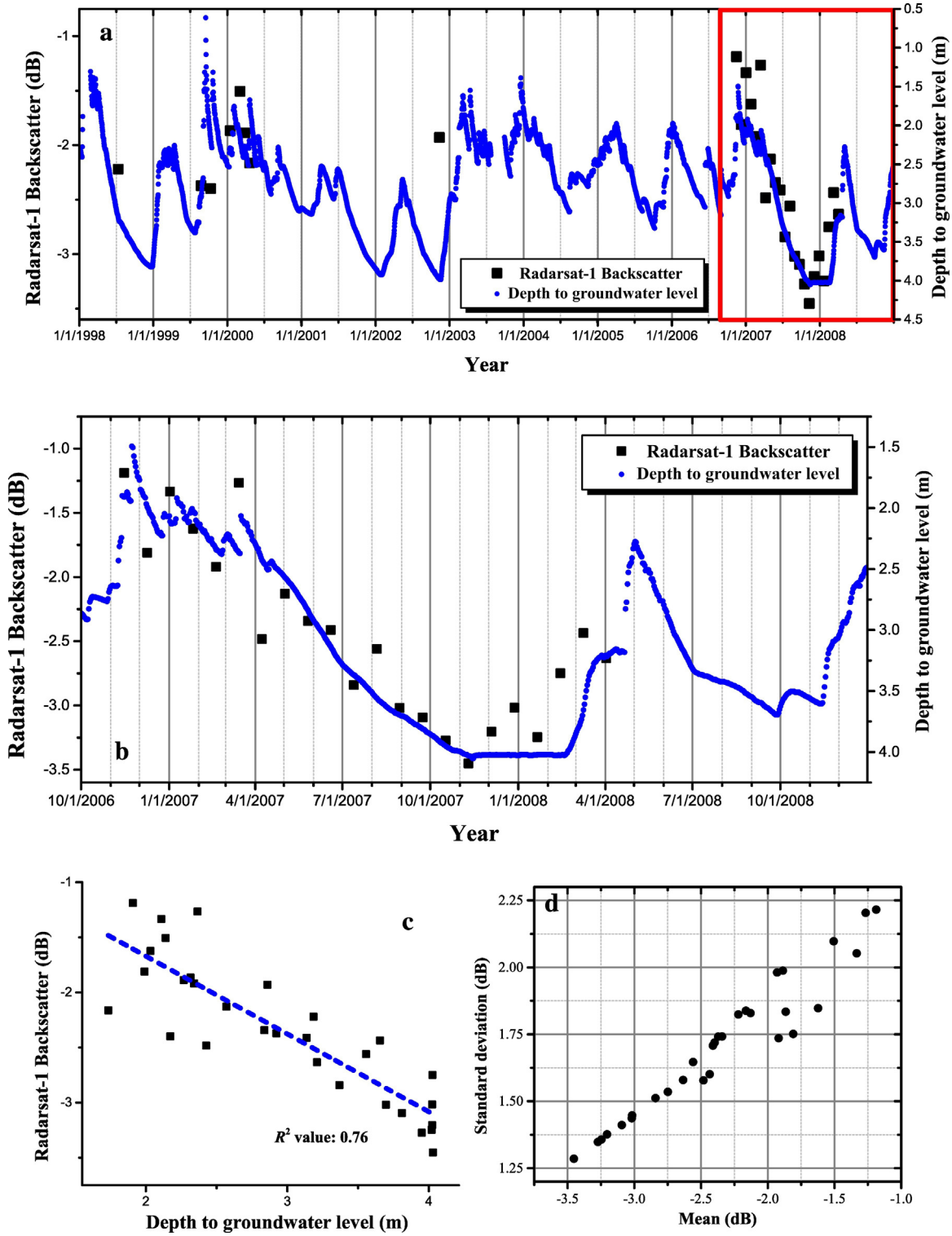

Fig. 4. Comparison between groundwater level and averaged Radarsat-1 SAR intensity from (a) 1998 to 2008, and (b) 2006 to 2008 (red box in panel (a)). (c) Linear regression of groundwater level and Radarsat-1 backscatter. (d) Scatter plot of average and standard deviation of Radarsat-1 SAR intensity (R-squared value: 0.93 significant at $p < 0.0001$, n: 30, ε: 0.07, intercept: 2.62 ± 0.10 (95% confidence), slope: 0.39 ± 0.04 (95% confidence)). (For interpretation of the references to color in this figure legend, the reader is referred to the web version of this article.)

Cypress Gum, Maple Gum, Pine Pocosin). This consistency means that L-band SAR intensity has better penetration capability over the vegetated wetland and most of the SAR returns persistently come from the subsurface soil column, which can be used to estimate soil moisture in areas populated by Atlantic White Cedar and Pine Pocosin. Even Upland Pine, which prospers in the levee area on the western edge of the GDS, and is not influenced by the surface water, has a higher R-squared value of 0.62 for ALOS PALSAR intensity. The disturbed fire, as expected, has the lowest value of 0.20 for PALSAR intensity. L-band SAR intensity is thus better suited to finding a close relationship with soil moisture content and can exclude the effect of seasonal standing surface water when vegetation maps are used in conjunction with intensity data.

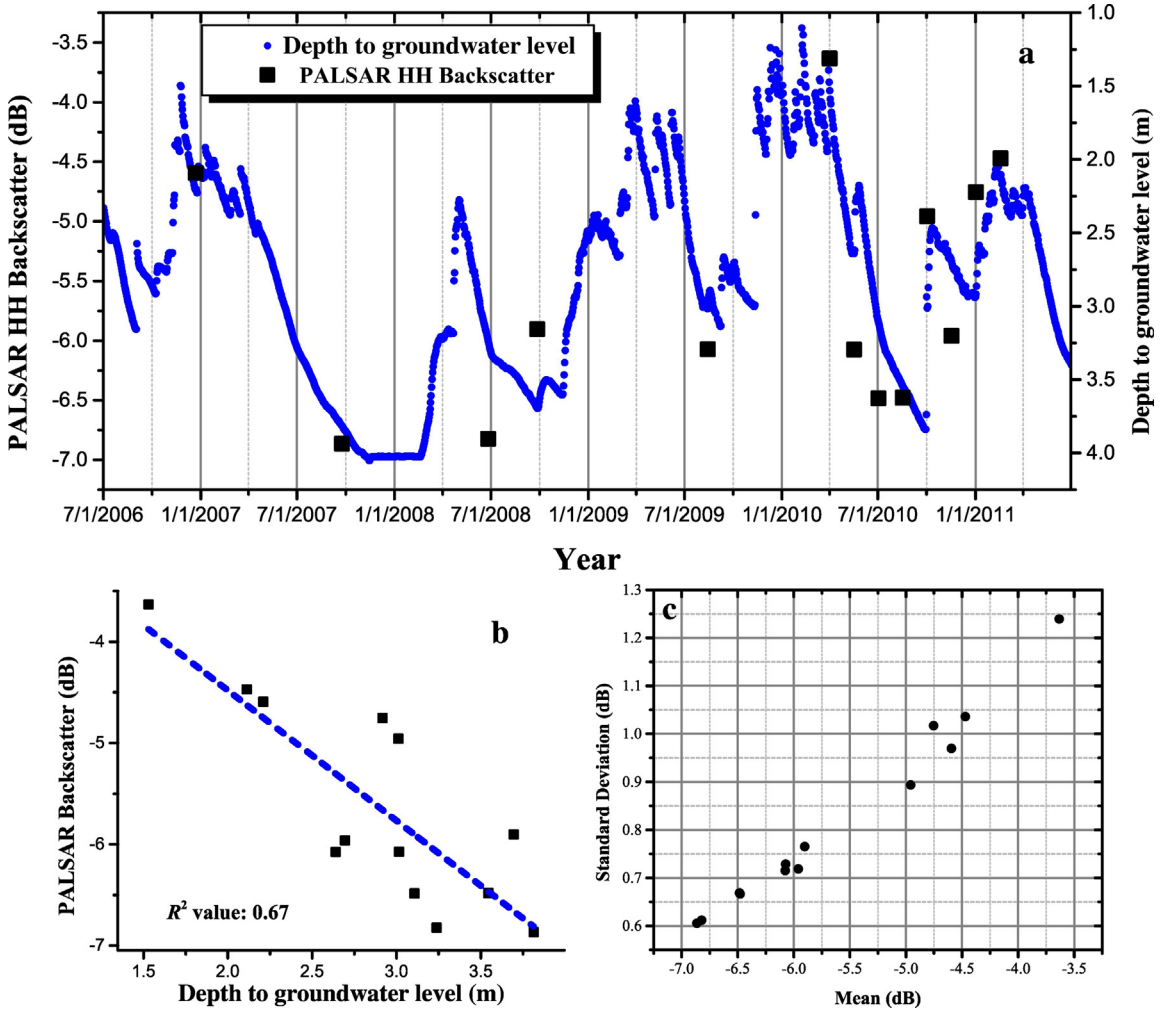

Fig. 5. (a) Comparison between groundwater level and average ALOS PALSAR intensity from 2006 to 2011. (b) Linear regression of groundwater level and ALOS PALSAR backscatter. (c) Scatter plot of average and standard deviation of ALOS PALSAR intensity (R-squared value: 0.98 significant at $p < 0.0001$, n: 13, ε: 0.03, intercept: 1.88 ± 0.11 (95% confidence), slope: 0.19 ± 0.02 (95% confidence)).

4.3. Extracting the inundated area from InSAR coherence

InSAR coherence can be used to characterize the hydrologic conditions related to inundation in the GDS, but because C-band Radarsat-1 did not maintain high coherence in the swamp, we focused on the L-band ALOS PALSAR datasets. Coherence observations over wetlands (e.g., Lu and Kwoun, 2008) differ greatly between wet and dry seasons, so the SAR signals acquired in different seasons do not exhibit consistent backscattering. Considering that the GDS is nearly dried out during summer, the InSAR coherence from SAR datasets between wet and dry season was insignificant. When we calculated InSAR coherence from SAR datasets acquired in the wet season, we found that areas subject to double-bounce scattering had high coherence (Fig. 7(a, b)). Although the InSAR coherence observations from two different periods (04/01/2010 to 10/02/2010 and 10/02/2010 to 02/17/2010) present little spatial difference, the maps consistently indicate that the western and northern regions of the GDS were exposed to double-bounce scattering. We extracted those areas with high coherence using the threshold of 0.35, which was iteratively and empirically determined (Fig. 7(c, d)). We anticipate that the areas prone to double-bounce scattering during wet season were flooded by the elevated surface water level and run-off events. These high-coherence maps (Fig. 7(c, d)) approximate the extent of inundation. From the maps, we can see the ditches disrupt water movement across the western swamp. The southeastern area is also observed to be relatively dry, even in the wet season, because the ditches and canals capture eastward water coming from the wetlands. However, determining the flooded areas based on the empirical coherence threshold requires further refinement and validation when the ground-truth information through field survey or other supplementary remote techniques is available. We aimed to extract the non-inundated areas in the GDS, rather than those subject to seasonal surface water impoundment, for comparison of the soil moisture with the InSAR products. In this way, we can minimize the effect of the seasonal run-off events on the SAR/InSAR products.

4.4. Estimating the surface water level changes in the inundated areas and groundwater level changes from InSAR time-series

In the areas with high InSAR coherence, the interferometric phase measurements can be related to relative water level changes in the forested wetland and soil moisture changes in the Pine Pocosin (communities of shorter vegetation, pines and shrubs). Due to double-bounce scattering in inundated areas, centimeter-level water level changes beneath the forest canopy can be detected (Fig. 8(a, b)). Lines of a–a', b–b', and c–c' are located in the areas where water run-off from ditches overflows onto the flat wetland, and their profiles show the variations in water level along their distances (Fig. 8(c)). The relative water level changes along line a–a' from 04/01/2010 to 10/02/2010 decreased, and those along line b–b' and c–c' between 11/17/2010 and 02/17/2011 increased. Points a, b', and c' are located at sites close to the

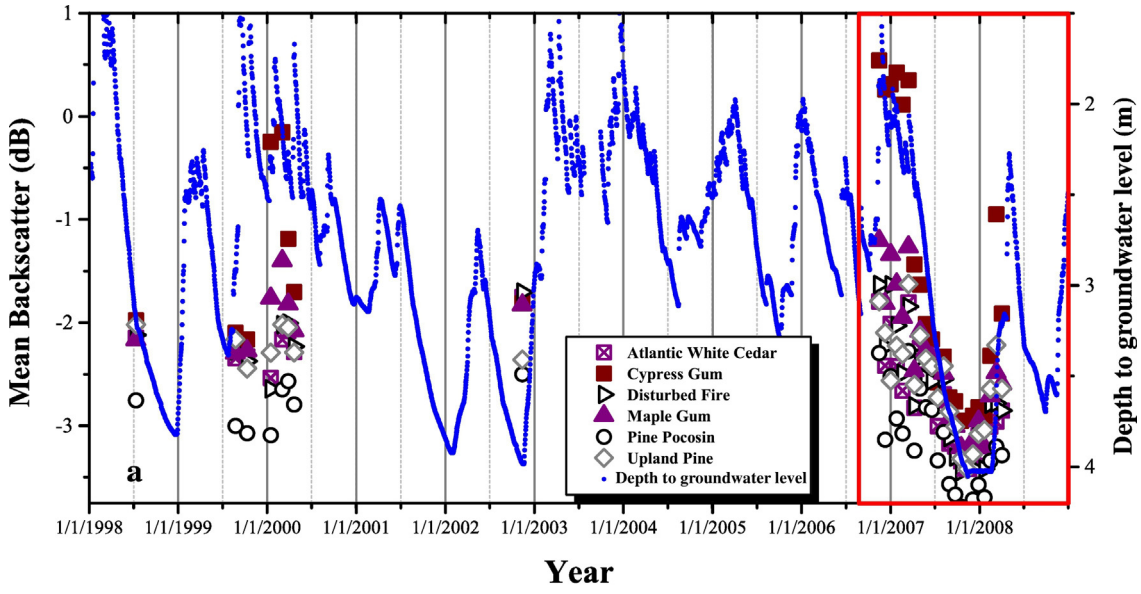
Mean Backscatter (dB)
Depth to groundwater level (m)
Year
a
Atlantic White Cedar
Cypress Gum
Disturbed Fire
Maple Gum
Pine Pocosin
Upland Pine
Depth to groundwater level
1/1/1998
1/1/1999
1/1/2000
1/1/2001
1/1/2002
1/1/2003
1/1/2004
1/1/2005
1/1/2006
1/1/2007
1/1/2008

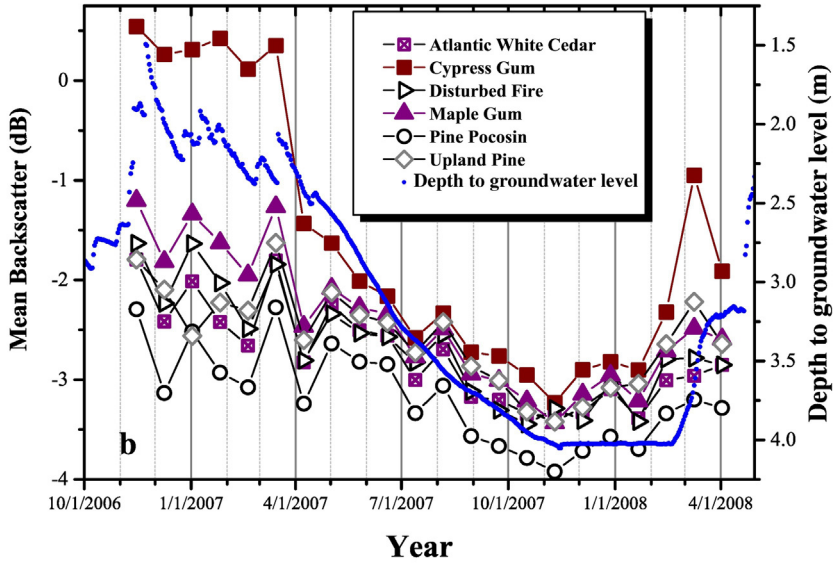
Mean Backscatter (dB)
Depth to groundwater level (m)
Year
b
Atlantic White Cedar
Cypress Gum
Disturbed Fire
Maple Gum
Pine Pocosin
Upland Pine
Depth to groundwater level
10/1/2006
1/1/2007
4/1/2007
7/1/2007
10/1/2007
1/1/2008
4/1/2008

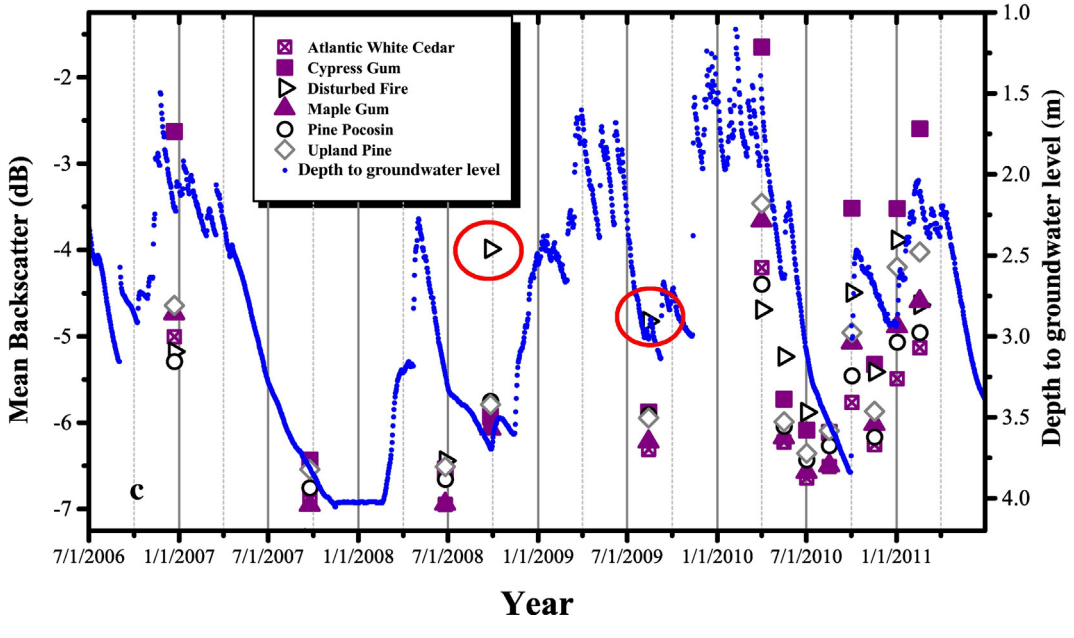
Mean Backscatter (dB)
Depth to groundwater level (m)
Year
c
Atlantic White Cedar
Cypress Gum
Disturbed Fire
Maple Gum
Pine Pocosin
Upland Pine
Depth to groundwater level
7/1/2006
1/1/2007
7/1/2007
1/1/2008
7/1/2008
1/1/2009
7/1/2009
1/1/2010
7/1/2010
1/1/2011

incoming water from ditches, and their nearby areas have large relative water level changes during the wet season. The southeastern area (red box in Fig. 8(b)) is not affected by surface water, but the interferometric results over the non-inundated areas can be associated with changes in soil moisture induced by changes in the groundwater level. Although the interferogram of Fig. 8(b) could keep high spatial coherence over the Pine Pocosin dominated areas (red box), most remaining InSAR pairs have low coherence due to the lack of stagnant surface water in the vegetation. We therefore need to introduce the concept of point-target scatterers that exhibit strong and persistent backscattering returns for estimating time-series surface changes induced by seasonally saturated soils.

With InSAR time-series measurements from 5 image pairs of 05/17/2010 to 07/02/2010, 07/02/2010 to 08/17/2010, 10/02/2010 to 11/17/2010, 11/17/2010 to 02/17/2010, and 01/02/2011 to 02/17/2011, we can estimate the vertical component of motion from the projection of line-of-sight (LOS) InSAR measurements to a vertical plane calculated from the satellite incidence angle, using the SBAS approach. Unfortunately, the southeastern area, mostly covered by short vegetation, could not maintain high coherence in our SAR datasets. More InSAR pairs can make our solution more rigorous while suppressing error components, but we could only select 5 due to this limited coherence. Before applying the SBAS method, we initially extracted Persistent Scatterer (PS) points over the whole GDS. The PS points with consistently strong backscatter and high coherence can be introduced as a reference in the case that the in situ information is insufficient. We calculated the amplitude dispersion index using the equation:

$$D_a = \frac{\sigma_a}{\overline{a}} \tag{4}$$

where σ_a and $\overline{a}$ is the standard deviation and mean of the time-series SAR amplitudes, respectively. From the initial PS points we selected those with small amplitude dispersion indexes and high average coherence (Fig. 9(a)). Because we only focus on the southeastern area, the PS points in other regions, which are influenced by surface water, are not considered for this analysis. To choose the final PS points, we assumed that elevated areas will have less groundwater level changes compared to nearby low-lying wetlands, because the localized peaks (i.e. tree islands under non-fluvial condition) are less sensitive to fluctuations of groundwater level and the low-lying areas will be more impounded by the ground water (Gusyev and Haitjema, 2011). A 30 m resolution digital elevation model (DEM), such as shuttle radar topography mission (SRTM), is not sufficient for picking the local elevation peak, and we instead used a light detection and ranging (LiDAR) DEM with 1.5 m resolution. We then picked a single PS point (red dot in Fig. 9(b)) that is characterized by low amplitude dispersion, high average InSAR coherence, and high elevation and additionally, is located near the groundwater measurement well (cyan triangle in Fig. 9(b)). The groundwater level changes at this well site are calculated using a time-series method. Because we selected this PS point based on high InSAR coherence from limited InSAR pairs, the coherence values are rather constant (>0.3) throughout a short acquisition period (May 2010–Feb 2011). Moreover, the temporal change of InSAR coherence for this point can be mostly attributed to the variation in perpendicular baselines between InSAR pairs. The InSAR coherence was only used as a threshold to identify PS points in this Pine Pocosin community.

5. Discussion

The hydrologic change in the GDS is a key driver of changes in the C- and L-band SAR intensity. Other effects, including aboveground biomass, tree structure, canopy openings, and vegetation density should not be disregarded, but the high correlation between SAR intensity and groundwater level change (Figs. 4, 5) shows that transmitted SAR signals are mostly influenced by double-bounce scattering in the inundated areas and the variation of soil moisture content over non-inundated regions. From ALOS PALSAR HV polarized datasets, which are supposed to be sensitive to the surface and volume scattering of the forest canopy, we could not find a meaningful relationship between two parameters (i.e., SAR backscattering intensity vs groundwater level). HH polarized SAR signals from Radarsat-1 and ALOS PALSAR could, however, penetrate the forest canopy and obtain echoes from the ground surface. Even though the penetration depth to soil layers in the swamp is on the order of sub-wavelength, the changes in groundwater levels can drive variations in the soil moisture, which, in turn, modify the SAR backscattering intensity.

Previous studies have been successfully conducted on the correlation of C- or L-band SAR backscatter and aboveground biomass or soil moisture in wetlands (Kasischke et al., 2003, 2009, 2011), but HH polarized SAR backscatter and long-term soil moisture in a wetland could not be thoroughly analyzed due to the limited observations of moisture contents in a soil layer. With the aid of the spaceborne soil moisture datasets from SMAP, the results from our study showed that HH polarized SAR backscatter has a close relationship with groundwater level changes and ultimately soil moisture changes. Cross-polarized (HV, VH) SAR signals can be more sensitive to the biophysical parameters (i.e. aboveground biomass) on the surface of wetlands (Kasischke et al., 2011) due to their scattering characteristics, including the mixed (volumetric) effects of vegetation and soils. On the other hand, our findings indicate that co-polarized (HH) SAR signals from Radarsat-1 and ALOS PALSAR are more influenced by soil moisture contents due their larger penetration depth in vegetated wetlands. Our results also agree well to a previous study that found positive correlations between co-polarized (VV) ERS SAR backscatter and soil moistures in vegetated Alaskan wetlands (Kasischke et al., 2009). Like the Alaskan wetlands (Kasischke et al., 2009), across the GDS increases in the water table correspond to an increase in a soil moisture and surface soil inundation, which results in the increase of SAR backscatter. It can be argued that the increased co-polarized SAR intensity is completely attributed to the double-bounce scattering in forested swamp. Because the SAR intensity over the Cypress Gum, which is the seasonally inundated association, was highly sensitive to the hydrologic changes, the argument can be partially true. During high water season (winter), many parts (mostly forested by Cypress Gum) of the GDS are covered by standing water. Therefore, using a vegetation cover map (Fig. 1(b)), we had to distinguish the effects of standing water from the variations in soil moisture to properly estimate the correlation between SAR backscatter and soil moisture contents. The SAR intensities over non-inundated (Pine Pocosin in the southeastern GDS) and occasionally inundated (Maple Gum) communities maintain high correlation with groundwater level changes (Fig. 6), implying that the soil moisture is influential on the backscattering of SAR signal. When water table remains low in the low water season (summer), SAR backscatters over the organic soils of peatlands are also low due to the reduced reflection from soil layers. However, increasing water table during high water season (winter) leads to the increase of moist soils as well as SAR backscatter. Nevertheless, the vegetation moisture content itself should not be ignored. The increased moisture content in the vegetation during the wet season can similarly affect the SAR intensity. With only the single polarized SAR datasets, it is difficult to distinguish the two effects of vegetation and soil saturation. Additionally, the wet season around January 2008 was the driest in the past 10 years, as indicated by the groundwater level (Fig. 6(a)).

Fig. 6. Comparison between groundwater level and average Radarsat-1 SAR intensity averages by vegetation types, from (a) 1998 to 2008, and (b) 2006 to 2008 (red box in panel (a)). (c) Comparison between groundwater level and ALOS PALSAR intensity by vegetation types. (For interpretation of the references to color in this figure legend, the reader is referred to the web version of this article.)

Table 1
R^2 values and regression results of SAR backscatters according to vegetation covers vs groundwater level.

Vegetation cover	R^2 values and regression results (95% confidence) SAR backscatter vs groundwater		
	Radarsat-1 backscatter (1998–2008) (n: 30)	Radarsat-1 backscatter (2006–2008) (n: 22)	ALOS backscatter (n: 13)
Atlantic White Cedar	0.49 ($p < 0.02$, ε: 0.36, intercept: -1.30 ± 0.53, slope: -0.44 ± 0.17)	0.76 ($p < 0.004$, ε: 0.25, intercept: -1.05 ± 0.46, slope: -0.54 ± 0.14)	0.69 ($p < 0.002$, ε: 0.47, intercept: -2.99 ± 1.35, slope: -1.02 ± 0.46)
Cypress Gum	0.63 ($p < 0.004$, ε: 0.75, intercept: 2.01 ± 1.11, slope: -1.19 ± 0.36)	0.81 ($p < 0.001$, ε: 0.59, intercept: 3.18 ± 1.10, slope: -1.53 ± 0.34)	0.69 ($p < 0.002$, ε: 0.99, intercept: 1.54 ± 2.85, slope: -2.18 ± 0.96)
Disturbed Fire	0.50 ($p < 0.004$, ε: 0.39, intercept: -1.10 ± 0.57, slope: -0.48 ± 0.19)	0.77 ($p < 0.001$, ε: 0.28, intercept: -0.73 ± 0.51, slope: -0.62 ± 0.16)	0.20 ($p < 0.02$, ε: 1.09, intercept: -3.07 ± 3.13, slope: -0.79 ± 1.06)
Maple Gum	0.67 ($p < 0.004$, ε: 0.37, intercept: -0.39 ± 0.54, slope: -0.64 ± 0.17)	0.84 ($p < 0.001$, ε: 0.27, intercept: -0.00 ± 0.51, slope: -0.77 ± 0.16)	0.69 ($p < 0.004$, ε: 0.60, intercept: -1.98 ± 1.72, slope: -1.30 ± 0.58)
Pine Pocosin	0.47 ($p < 0.02$, ε: 0.34, intercept: -1.92 ± 0.49, slope: -0.34 ± 0.16)	0.66 ($p < 0.004$, ε: 0.29, intercept: -1.65 ± 0.53, slope: -0.49 ± 0.17)	0.60 ($p < 0.004$, ε: 0.47, intercept: -3.36 ± 1.35, slope: -0.84 ± 0.46)
Upland Pine	0.52 ($p < 0.02$, ε: 0.32, intercept: -1.26 ± 0.47, slope: -0.41 ± 0.15)	0.62 ($p < 0.004$, ε: 0.31, intercept: -1.07 ± 0.57, slope: -0.48 ± 0.18)	0.62 ($p < 0.004$, ε: 0.67, intercept: -1.83 ± 1.91, slope: -1.24 ± 0.17)

The hydrologic input for the wet season and hydroperiod is crucial for maintaining the appropriate soil moisture in peatlands throughout the year. The decreased soil moisture leaves the wetland vulnerable to wildfires and we see this manifest with the severe wildfire that occurred in June of 2008 and lasted for four months. Time-series of SAR intensities, that we found can alternatively replace the groundwater level measurements, are extremely valuable for evaluating the risk of the wildfire hazard.

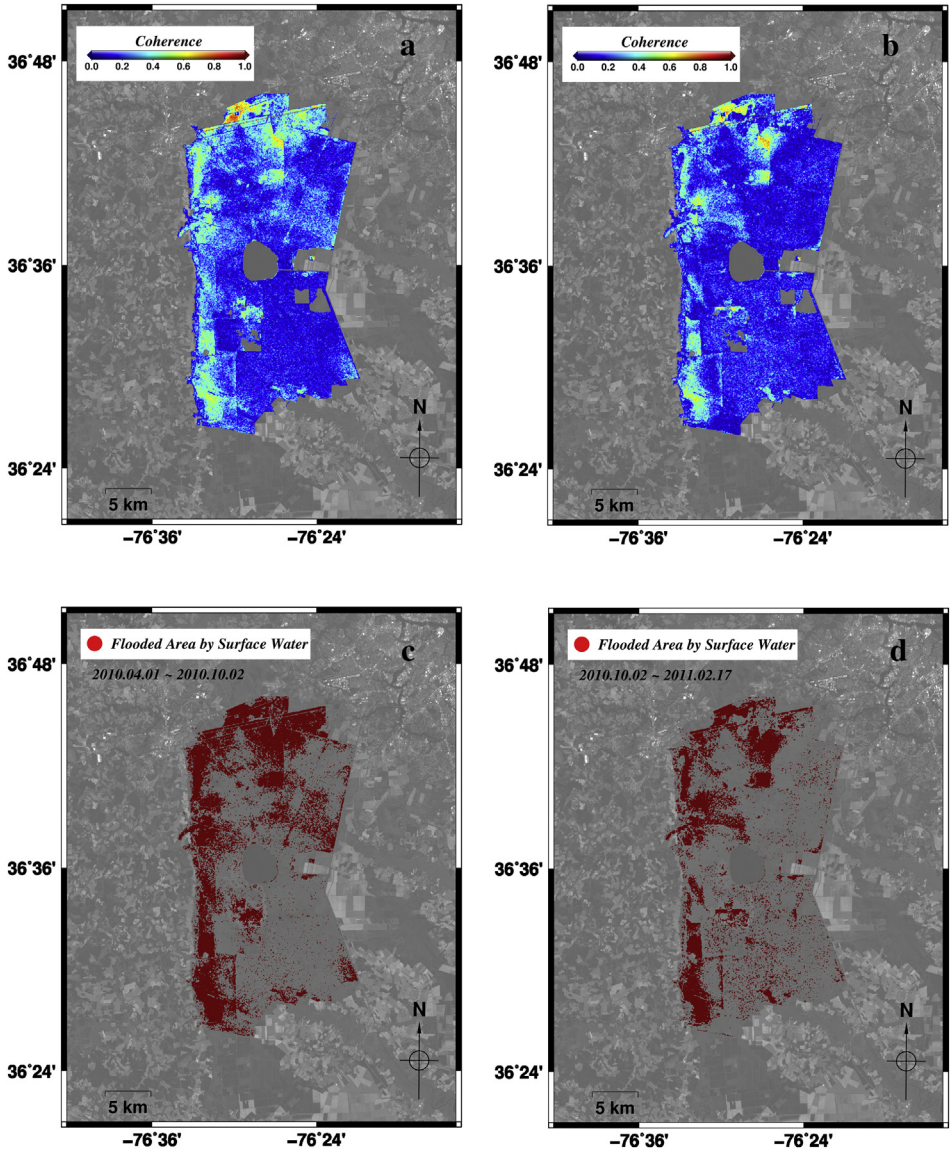

Fig. 7. InSAR coherence maps during (a) 2010.04.01 and 2010.10.02, and (b) 2010.10.02 and 2011.02.17. Inundation area estimated from InSAR coherence from the pairs of (c) 2010.04.01 and 2010.10.02, and (d) 2010.10.02 and 2011.02.17.

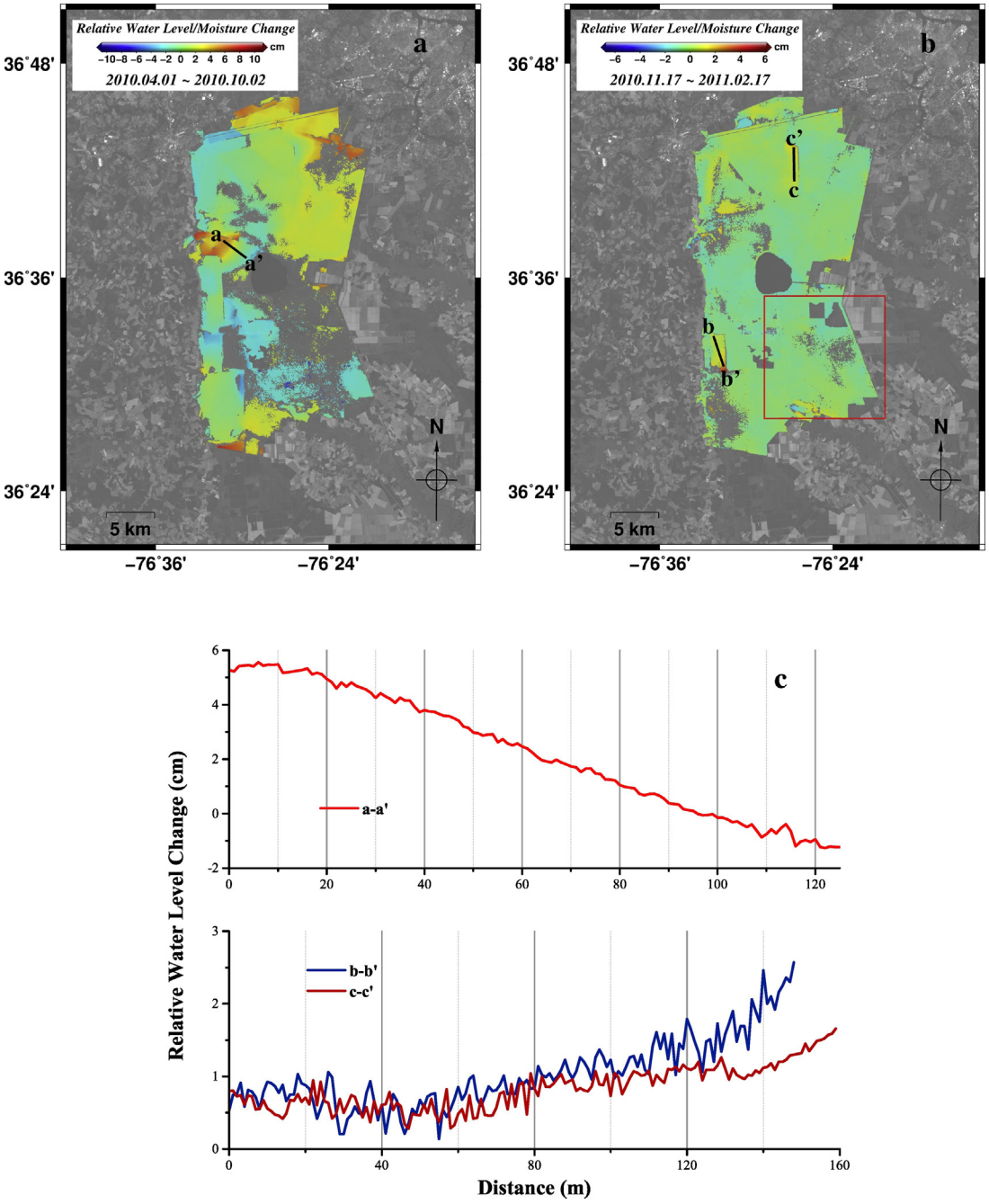

Fig. 8. Relative water level change (soil moisture change) map from a pair of (a) 2010.04.01–2010.10.02 and (b) 2010.11.17–2011.02.17. (c) Relative water level change of profile a-a', b-b', and c-c'. (For interpretation of the references to color in this figure, the reader is referred to the web version of this article.)

We can delineate the inundated and non-inundated areas using the InSAR coherence, because high coherence is achieved in the forested swamp under the influence of double-bounce scattering. The flooding map during wet season (Fig. 7) can provide useful information for characterizing the wetland, when comparing it with the vegetation cover map (Fig. 1). The most dominant vegetation community in the swamp was the Cypress Gum before the development of the GDS began in 18th century. As seen in the lower part of Fig. 7(c) and (d), the human-made ditches interrupt the natural water movement from west to east. The eastern part of the inundated areas, including areas damaged by the 2008 and 2011 wildfires, remained drier compared to the undisturbed condition where the natural sheet flows saturate the region. The dry condition along with selective logging triggered the transformation of the vegetation community from Cypress Gum to Maple Gum. In the western part, which is often flooded by standing water during the wet season, the Cypress Gum could still prosper. However, the eastern part across the inundated area is currently dominated by the Maple Gum, and it is further expanding its community over the GDS due to human-made waterways and ditches providing drainage that decreases soil moisture.

The relative surface water level changes can be measured using InSAR techniques outlined in this study, and the results could be used to monitor hydrologic changes in the inundated area and identify the location of the water inflow (Fig. 8). In the dissected wetlands, these InSAR methods indicate that water levels rise or drop unevenly with the spatial gradient of relative water level changes (Fig. 8(a, b)).

Contrary to the Everglades in Florida, there are no water level gages located inside the swamp of our study area. This restricts the capability

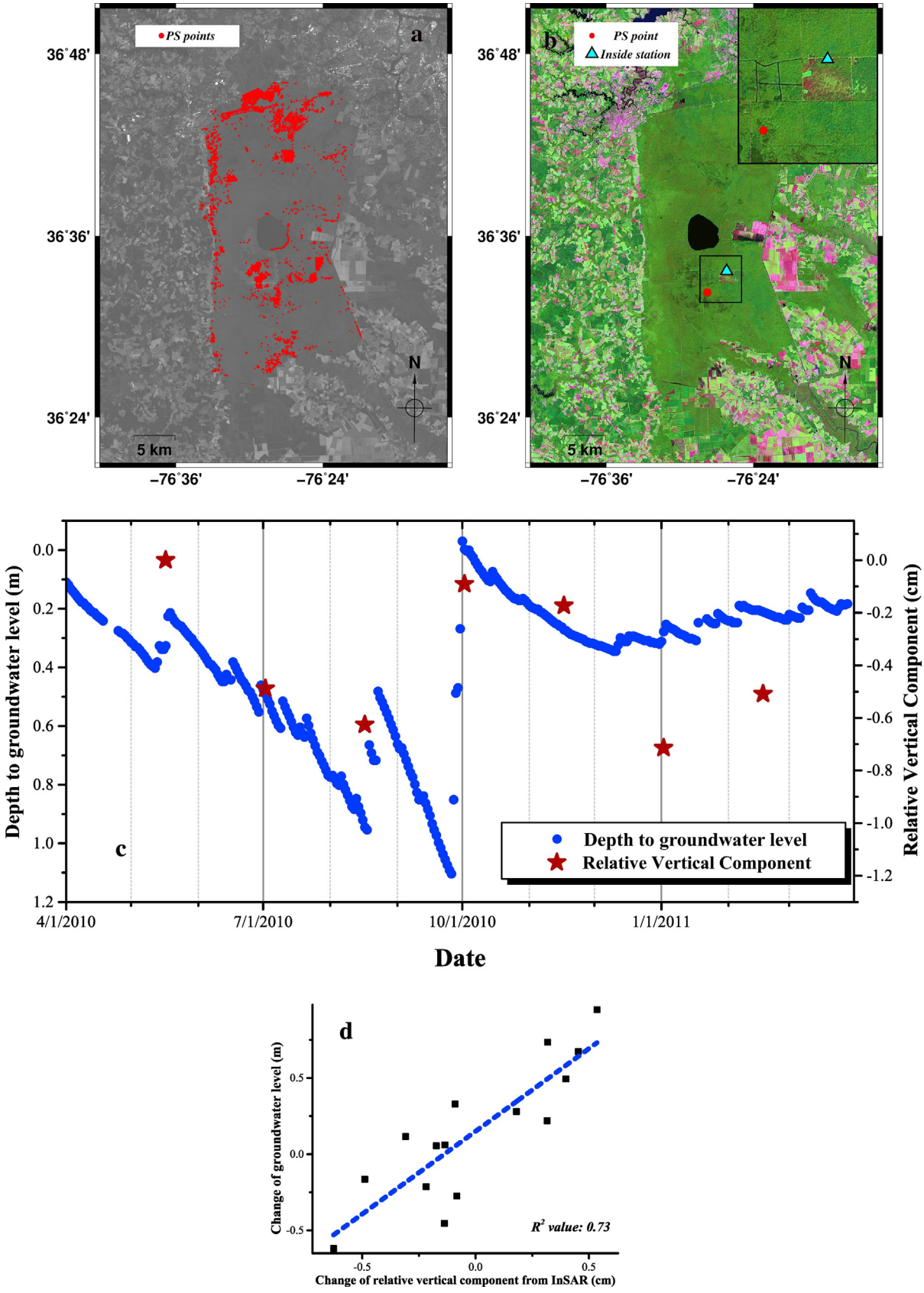

Fig. 9. (a) Initial PS points, which were extracted from time-series InSAR measurements. (b) Selected PS point (red dot) and location of groundwater well site (cyan triangle). (c) Comparison of retrieved vertical components from time-series InSAR measurements and groundwater level. (d) Linear regression of the changes of groundwater level and relative vertical component from InSAR between two SAR acquisition dates (R-squared value: 0.73 significant at $p < 0.002$, n: 15, ε: 0.24, intercept: 0.15 $\pm$ 0.13 (95% confidence), slope: 1.09 $\pm$ 0.40 (95% confidence)). (For interpretation of the references to color in this figure legend, the reader is referred to the web version of this article.)

to continuously monitor the water level fluctuations and evaluate the hazard risk induced by the abrupt run-off and flooding. We have shown that InSAR can help estimate the long-term hydrologic changes with high spatial resolution when local ground based measurements are unavailable. Furthermore, when we can create a time-series from InSAR measurements, we can indirectly estimate the soil moisture content from groundwater level. Based on the assumption that the PS points are stable and do not have a significant groundwater level change, we can also calculate vertical motion using this InSAR time-series approach (Fig. 9(c)). However, the coherence from InSAR pairs related to Jan 2 of 2011 acquisition during the wettest season is relatively low compared to other InSAR pairs, because the wet condition in the peatland altered the scattering characteristics and disturbed the consistent phase measurements. The changes in groundwater level and vertical component retrieved from InSAR pairs between two SAR acquisition dates, excluding the relatively low coherence InSAR pairs, have a close relationship (Fig. 9(d); R-squared value: 0.73). Because we have only a single groundwater well inside the peatland and the InSAR coherence is often lost throughout years, we cannot extend our comparison between the changes in groundwater level and interferometric phase measurement to a large spatio-temporal scale. However, based on the limited comparison between two parameters, the vertical movements from InSAR appear to have high correlation with the groundwater level changes (Fig. 9(d)) and also therefore the variations in soil moisture content. If the average SAR intensity can be used to find the relationship with groundwater level changes in the reduced resolution, then the InSAR time-series method could be utilized to characterize the variation in the water table at pin-pointed locations. The main limitation was found to be poor InSAR coherence when temporal separations of the SAR images are too long and the vegetation conditions change between leaf-on and leaf-off seasons. In the large scale, where averaging SAR intensity over the entire GDS was performed, the seasonal vegetation effect was ignorable. However, in the small scale over the Pine Pocosin communities, the seasonal vegetation changes can still affect our InSAR time-series results.

6. Conclusion

The GDS is a peatland with a long history of development. Although hydrologic change is crucial for conserving the peatland, its dynamics have not been thoroughly unveiled by the use of remote sensing technology, especially radar sensors. Our SAR observations can characterize the seasonal hydrologic changes, delineate the inundated area, measure the relative surface water level changes in the inundated area, and estimate the changes in groundwater levels based on the close relationship discovered in this study between the SMAP soil moisture and local groundwater table measurements. Our study shows the possibility that soil moisture changes can be detected by the averaged SAR intensity and InSAR time-series method. Our results partially explain the transformation of vegetation in the GDS as a result of the dried soils created by the effects of anthropogenic drainage features such as ditches and canals and the wildfire that occurred in 2008.

Future studies cannot be completed without more extensive and detailed field measurements of soil moisture, biomass, and surface water level changes in the GDS. Even without the “ground-truth” measurements, we live in the wake of new advanced radar sensors including SMAP, C-band Sentinel-1A/B, L-band ALOS-2 PALSAR-2, and upcoming S/L-band NISAR (NASA-ISRO SAR Mission). SMAP particularly, can supply the reference information about soil moisture from space, and high-resolution SAR data can supplement the passive radar sensor (radiometer) of SMAP as was originally planned for that mission. In addition, SAR sensors with full polarization (HH, HV, VH, VV) will enhance our understanding of vegetation structure, biomass, and even soil moisture. Advancements in the capabilities and data products provided by SAR sensors may eventually provide information like that presented in this study, but until then, the techniques used here to observe complicated associations and processes in wetland hydrology can be used to better understand and thus preserve the sensitive ecosystems of our vanishing peatlands.

Acknowledgements

Radarsat-1 SAR data are copyrighted by the Canadian Space Agency (CSA) (1998–2008) and ALOS PALSAR data are copyrighted by JAXA/METI (2006–2011). Both datasets were provided by the Alaska Satellite Facility (ASF). SMAP soil moisture data were obtained through NASA's Earth Observing System Data and Information System (EOSDIS) and National Snow and Ice Data Center (NSIDC). The groundwater level and precipitation data were obtained from http://maps.waterdata.usgs.gov/mapper/index.html. The LiDAR DEM was obtained from Virginia Lidar (http://virginialidar.com). We appreciate the kind support of Susan Hazlett, Dianna Hogan, and Gary Speiran from USGS on land cover map and other information over the GDS. We also thank to the kind help of Kimberly Degrandpre in our department to proofread this manuscript, and Dr. Eric S. Kasischke (associate editor of Remote Sensing of Environment)'s thorough and constructive comments to improve our approach and analysis. Most geocoded images were drawn by the Generic Mapping Tools (GMT). This work was supported by USGS Biologic Carbon Sequestration Program (G14AC00152) and Shuler-Foscue Endowment at Southern Methodist University.

References

Alsdorf, D., Melack, J., Dunne, T., Mertes, L., Hess, L., Smith, L., 2000. Interferometric radar measurements of water level changes on the Amazon floodplain. Nature 404, 174–177.
Alsdorf, D., Smith, L., Melack, J., 2001. Amazon floodplain water level changes measured with interferometric SIR-C radar. IEEE Trans. Geosci. Remote Sens. 39, 423–431.
Berardino, P., Fornaro, G., Lanari, R., Sansosti, E., 2002. A new algorithm for surface deformation monitoring based on small baseline differential SAR interferograms. IEEE Trans. Geosci. Remote Sens. 40 (2375–238).
Bradley, K.C., 2013. The Great Dismal Swamp: A Twentieth-century Perspective. (Master Thesis). American University, Washington, D.C.
Brisco, B., Ahern, F., Murnaghan, K., White, L., Canisus, F., Lancaster, P., 2017. Seasonal change in wetland coherence as an aid to wetland monitoring. Remote Sens. 9 (2): 158. http://dx.doi.org/10.3390/rs9020158.
Brodzik, M.J., Billingsley, B., Haran, T., Raup, B., Savoie, M.H., 2012. EASE-Grid 2.0: incremental but significant improvements for earth-gridded datasets. ISPRS Int. J. Geo-Inf. 3 (3), 1154–1156.
Carter, V., Garrett, M.K., Shima, L., Gammon, P., 1977. The great dismal swamp: management of a hydrologic resource with the aid of remote sensing. J. Am. Water Resour. Assoc. 13 (1), 1–12.
Day, F.P., 1982. Litter decomposition rates in the seasonally flooded Great Dismal Swamp. Ecology 63 (3), 670–678.
Day, F.P., West, S.K., Tupacz, E.G., 1988. The influence of ground-water dynamics in a periodically flooded ecosystem, the Great Dismal Swamp. Wetlands 8 (1). http://dx.doi.org/10.1007/BF03160805.
De Zan, F., Parizzi, A., Prats-Iraola, P., López-Dekker, P., 2014. A SAR interferometric model for soil moisture. IEEE Trans. Geosci. Remote Sens. 52 (1), 418–425.
Dise, N.B., 2009. Peatland response to global change. Science 326 (5954):810–811. http://dx.doi.org/10.1126/science.1174268.
Dubois, P.C., van Zyl, J., Engman, T., 1995. Measuring soil moisture with imaging radars. IEEE Trans. Geosci. Remote Sens. 33 (4):915–926. http://dx.doi.org/10.1109/36.406677.
Fenner, N., Freeman, C., 2011. Drought-induced carbon loss in peatlands. Nature 4: 895–900. http://dx.doi.org/10.1038/ngeo1323.
Fleming, G., Coulling, P., Walton, D., McCoy, K., Parrish, M., 2001. The natural communities of Virginia: classification of ecological community groups, first approximation. Natural Heritage Technical Report 01-1. Virginia Department of Conservation and Recreation, Division of Natural Heritage, Richmond (Unpublished report).
Franceschetti, G., Migliaccio, M., Riccio, D., Schirinzi, G., 1992. SARAS: a SAR raw signal simulator. IEEE Trans. Geosci. Remote Sens. 30, 110–123.
Gusyev, M., Haitjema, H.M., 2011. Modeling flow in wetlands and underlying aquifers using a discharge potential formulation. J. Hydrol. 408, 91–99.
Harriss, R.C., Sebacher, D.I., Day, F.P., 1982. Methane flux in the Great Dismal Swamp. Nature 297:673–674. http://dx.doi.org/10.1038/297673a0.
Hess, L.L., Melack, J.M., Simonett, D.S., 1990. Radar detection of flooding beneath the forest canopy: a review. Int. J. Remote Sens. 11, 313–1325.
Hess, L.L., Melack, J.M., Filoso, S., Wang, Y., 1995. Delineation of inundated area and vegetation along the Amazon floodplain with the SIR-C synthetic aperture radar. IEEE Trans. Geosci. Remote Sens. 33, 896–904.
Hess, L.L., Melack, J.M., Novo, E.M.L.M., Barbosa, C.C.F., Gastil, M., 2003. Dual-season mapping of wetland inundation and vegetation for the central Amazon basin. Remote Sens. Environ. 87, 404–428.

Hutnick, R., Yawney, H., 1961. Silvical characteristics of red maple (*Acer rabrum*), Washington: Department of Agriculture, Forest Service. Station Paper 142. US Government Printing Office, p. 18.

Ise, T., Dunn, A.L., Wofsy, S.C., Moorcroft, P.R., 2008. High sensitivity of peat decomposition to climate change through water-table feedback. Nature 1:763–766. http://dx.doi.org/10.1038/ngeo331.

Joseph, A.T., van der Velde, R., O'Neill, P.E., Lang, R., Gish, T., 2010. Effects of corn on C-and L-band radar backscatter: a correction method for soil moisture retrieval. Remote Sens. Environ. 114 (11), 2417–2430.

Jung, H.C., Alsdorf, D., 2010. Repeat-pass multi-temporal interferometric SAR coherence variations with Amazon floodplain and lake habitats. Int. J. Remote Sens. 31 (4), 881–901.

Kasischke, E.S., Fowler, G.W., 1989. A statistical approach for determining radiometric presicions and accuracies in the calibration of synthetic aperture radar imagery. IEEE Trans. Geosci. Remote Sens. 27 (4), 416–427.

Kasischke, E.S., Smith, K.B., Bourgeau-Chavez, L.L., Romanowicz, E.A., Brunzell, S., Richardson, C.J., 2003. Effects of seasonal hydrologic patterns in south Florida wetlands on radar backscatter measured from ERS-2 SAR imagery. Remote Sens. Environ. 88, 423–441.

Kasischke, E.S., Bourgeau-Chavez, L.L., Rober, A.R., Wyatt, K.H., Waddington, J.M., Turetsky, M.R., 2009. Effects of soil moisture and water depth on ERS SAR backscatter measurements from an Alaskan wetland complex. Remote Sens. Environ. 113, 1868–1873.

Kasischke, E.S., Tanase, M.A., Bourgeau-Chavez, L.L., Borr, M., 2011. Soil moisture limitations on monitoring boreal forest regrowth using spaceborne L-band SAR data. Remote Sens. Environ. 115, 227–232.

Kim, J.-W., Lu, Z., Lee, H., Shum, C.K., Swarzenski, C., Doyle, T., Baek, S., 2009. Integrated analysis of PALSAR/Radarsat-1 InSAR and ENVISAT altimeter for mapping of absolute water level changes in Louisiana wetland. Remote Sens. Environ. 113 (11): 2356–2365. http://dx.doi.org/10.1016/j.rse.2009.06.014.

Kim, S.-W., Wdowinski, S., Amelung, F., Dixon, T.H., Won, J.-S., 2013. Interferometric coherence analysis of the Everglades wetlands, south Florida. IEEE Trans. Geosci. Remote Sens. 51 (12):5210–5224. http://dx.doi.org/10.1109/TGRS.2012.2231418.

Kim, J.-W., Lu, Z., Jones, J.W., Shum, C.K., Lee, H., Jia, Y., 2014. Monitoring Everglades freshwater marsh water level using L-band synthetic aperture radar backscatter. Remote Sens. Environ. 150, 66–81.

Kornelsen, K.C., Coulibaly, P., 2013. Advanced in soil moisture retrieval from synthetic aperture radar and hydrological applications. J. Hydrol. 476:460–489. http://dx.doi.org/10.1016/j.jhydrol.2012.10.044.

Kwoun, O.-I., Lu, Z., 2009. Multi-temporal RADARSAT-1 and ERS backscattering signatures of coastal wetlands in southeastern Louisiana. Photogramm. Eng. Remote. Sens. 75 (5), 607–617.

Laing, J.M., Shear, T.H., Blazich, F.A., 2011. How management strategies have affected Atlantic White cedar forest recovery after massive wind damage in the Great Dismal Swamp. For. Ecol. Manag. 262 (8), 1337–1344.

Le Hégarat-Mascle, S., Zribi, M., Alem, F., Weisse, A., Loumagne, C., 2002. Soil moisture estimation from ERS/SAR data: toward an operational methodology. IEEE Trans. Geosci. Remote Sens. 40 (12), 2647–2658.

Little, E., 1979. Checklist of United States trees (native and naturalized), Washington: US Department of Agriculture. Agriculture Handbook 541. US Government Printing Office, p. 375.

Lu, Z., Dzurisin, D., 2014. InSAR imaging of Aleutian volcanoes: monitoring a volcanic arc from space. Springer Praxis Books, Geophysical Sciences. Springer ISBN 978-3-641-00347-9. (390 pp.).

Lu, Z., Freymueller, J., 1998. Synthetic aperture radar interferometry coherence analysis over Katmai volcano group, Alaska. J. Geophys. Res. 103, 29887–29894.

Lu, Z., Kwoun, O., 2008. Radarsat-1 and ERS interferometric analysis over southeastern coastal Louisiana: implication for mapping water-level changes beneath swamp forests. IEEE Trans. Geosci. Remote Sens. 46 (4), 2167–2184.

Lu, Z., Meyer, D., 2002. Study of high SAR backscattering due to an increase of soil moisture over less vegetated area: its implication for characteristic of backscattering. Int. J. Remote Sens. 23 (6), 1065–1076.

Lu, Z., Crane, M., Kwoun, O., Wells, C., Swarzenski, C., Rykhus, R., 2005. C-band radar observes water-level change in swamp forests. Eos. Trans. AGU 86 (14), 141–144.

Lu, Z., Kim, J.W., Shum, C.K., 2014. Coastal wetlands: mapping by interferometric synthetic aperture radar (InSAR). Encyclopedia of Natural Resources. vol. 1. Taylor & Francis. ISBN: 9781439852583. http://dx.doi.org/10.1081/E-ENRL-120049157.

Mitsch, W.M., Hernandez, M.E., 2013. Landscape and climate change threats to wetlands of North and Central America. Aquat. Sci. 75, 133–149.

Moran, M.S., Hymer, D.C., Qi, J.G., Sano, E.E., 2000. Soil moisture evaluation using multitemporal synthetic aperture radar (SAR) in semiarid rangeland. Agric. For. Meteorol. 105 (1–3), 69–80.

NASA, 2014. SMAP (Soil Moisture Active Passive) Handbook: Mapping Soil Moisture and Freeze/Thaw From Space. Jet Propulsion Laboratory Publication, pp. 1–192.

Oh, Y., Sarabandi, K., Ulaby, F.T., 1992. An empirical model and an inversion technique for radar scattering from bare soil surfaces. IEEE Trans. Geosci. Remote Sens. 30 (2), 370–381.

Ramsey III, E.W., 1995. Monitoring flooding in coastal wetlands by using radar imagery and ground-based measurements. Int. J. Remote Sens. 16 (13), 2495–2502.

Ramsey III, E.W., Lu, Z., Rangoonwala, A., Rykhus, R., 2006. Multiple baseline radar interferometry applied to coastal land cover classification and change analyses. GIsci Remote Sens. 43 (4), 283–309.

Romshoo, S., Koike, M., Onaka, S., Oki, T., Musiake, K., 2002. Influence of surface and vegetation characteristics on C-band radar measurements for soil moisture content. J. Indian Soc. Remote Sens. 30 (4), 229–244.

Schmidt, D.A., Bürgmann, R., 2003. Time-dependent land uplift and subsidence in the Santa Clara valley, California, from a large interferometric synthetic aperture radar dataset. J. Geophys. Res. 108 (B9). http://dx.doi.org/10.1029/2002JB002267.

Schroeder, J.G., Taras, M.A., 1985. Atlantic white-cedar (*Chamaecyparis thyoides* (L.) B.S.P.), Washington, DC, USA. USDA Forest Service, FS-225.

Sleeter, R., Sleeter, B.M., Williams, B., Hogan, D., Hawbaker, T., Zhu, Z., 2017. A carbon balance model for the great dismal swamp ecosystem. Carbon Balance Manag. 12 (2). http://dx.doi.org/10.1186/s13021-017-0070-4.

Somorowska, U., 2003. Risk assessment of the occurrence of the extreme values of groundwater levels, discharge and soil moisture stages. Int. J. Ecohydrol. Hydrobiol. 3, 311–321.

Turetsky, M.R., Benscoter, B., Page, S., Rein, G., van der Werf, G.R., Watts, A., 2014. Global vulnerability of peatlands to fire and carbon loss. Nat. Geosci. 8, 11–14.

Ulaby, F.T., Moore, R.K., Fung, A.K., 1982. Microwave Remote Sensing: Active and Passive, Volume 2. Addison-Wesley Publishers, Reading, Mass.

USFWS (U.S. Fish & Wildlife Service), 2006. Great Dismal Swamp National Wildlife Refuge and Nansemond National Wildlife Refuge: Final Comprehensive Conservation Plan. Retrieved from. http://www.fws.gov/uploadedFiles/Region_5/NWRS/South_Zone/Great_Dismal_Swamp_Complex/Great_Dismal_Swamp/FinalCCP_GDS.pdf.

Wang, Y., Hess, L.L., Filoso, S., Melack, J.M., 1995. Understanding the radar back-scattering from flooded and nonflooded Amazonian forests: results from canopy backscatter modeling. Remote Sens. Environ. 54, 324–332.

Wdowinski, S., Amelung, F., Miralles-Wilhelm, F., Dixon, T., Carande, R., 2004. Space-based measurements of sheet-flow characteristics in the Everglades wetland, Florida. Geophys. Res. Lett. 31, L15503. http://dx.doi.org/10.1029/2004GL020383.

Wdowinski, S., Kim, S.-W., Amelung, F., Dixon, T., Miralles-Wilhelm, F., Sonenshein, R., 2008. Space-based detection of wetlands' surface water level changes from L-band SAR interferometry. Remote Sens. Environ. 112, 681–696.

Wigneron, J.P., Parde, M., Waldteufel, P., Chanzy, A., Kerr, Y., Schmidl, S., Skou, N., 2004. Characterizing the dependence of vegetation model parameters on crop structure, incidence angle, and polarization at L-band. IEEE Trans. Geosci. Remote Sens. 42 (2), 416–425.

Zwieback, S., Hensley, S., Hajnsek, I., 2015. Assessment of soil moisture effects on L-band radar interferometry. Remote Sens. Environ. 164, 77–89.